Synthesis and Ethylene Reactivity of Dinuclear Iron and Cobalt Complexes Supported by Macrocyclic Bis-(pyridine-diimine) Ligands Containing *Ortho*-terphenyl Linkers

Erik D. Reinhart and Richard F. Jordan*

Department of Chemistry, The University of Chicago, 5735 South Ellis Avenue, Chicago, IL 60637, United States

ABSTRACT: The synthesis and ethylene reactivity of a new family of dinuclear Co_2Br_4 and Fe_2Br_4 complexes supported by binucleating macrocyclic bis(pyridine-diimine) (PDI) ligands that contain 4,4''-R_2-3,3''-*ortho*-terphenyl linkers (**1**, R =H; **2**, R = Me; **3**, R = ^{i}Pr) are described. In the solid state, (**1**-**3**)M_2Br_4 (M = Zn, Fe, Co) adopt C_s-*skew*-*syn* structures in which the (PDI)M planes are skewed 49-82º relative to each other and both middle rings of the *ortho*-terphenyl bridges are on the same side of the molecule. The metal-metal distances range between 5.7600(8) and 6.232(1) Å. In solution, (**1**)M_2Br_4 (M = Zn, Co, Fe) undergo a fluxional process that permutes the two inequivalent (PDI)M units, while (**2**)M_2Br_4 and (**3**)M_2Br_4 are static and adopt C_s-symmetric structures similar to those observed in the solid state. Activation of (**2**)Fe_2Br_4 and (**3**)Fe_2Br_4 with MMAO-12 or triisobutylaluminum (TIBA) in the presence of ethylene generates catalysts that produce solid polyethylene (M_w = 4,500 to 280,000 Da), which contrasts with the reported production of α-olefins by analogous mononuclear (PDI)$FeCl_2$ catalysts. (**3**)Fe_2Br_4/TIBA and (**3**)Fe_2Br_4/MMAO-12 produce polyethylenes with broad molecular weight distributions (MWDs) due to chain transfer to Al. (**3**)Co_2Br_4/1,000 TIBA and (**3**)Co_2Br_4/1,000 MMAO-12 also produce polyethylenes with broad MWDs. However, in these cases chain transfer to Al is not operative and the broad MWDs result from multisite behavior.

INTRODUCTION

The ethylene polymerization behavior of pyridine-diimine (PDI) Fe and Co complexes activated by Al reagents (MAO or MMAO) was first reported by Brookhart and Gibson in the late 1990s.[1,2] These compounds exhibit very high activity in ethylene homopolymerization to produce linear polyethylene.[3–6] More recently, PDI metal complexes have been used in catalytic hydrosilylation,[7–10] hydroboration,[11–14] [2+2] cycloaddition,[15–18] CO_2/ethylene coupling,[19] and ring-opening polymerization of epoxides, lactide and caprolactone.[20–26] However, despite their high activities in ethylene polymerization, (PDI)Fe and (PDI)Co catalysts suffer from poor thermal stability at elevated temperatures and short catalyst lifetimes (often <15 min). One strategy that has been explored to improve the performance of (PDI)M catalysts is to incorporate the (PDI)M unit into a multinuclear structure using linear or macrocyclic bi- or polynucleating ligands.[27–34]

Chart 1 shows the structures of several multinuclear Fe and Co complexes supported by macrocyclic multinucleating PDI ligands that have been examined for ethylene polymerization. In the *anti*-double-decker complexes (**A**)M_2Cl_4 (M = Fe, Co) reported by Takeuchi, the two PDI planes are arranged in a parallel orientation and the MCl_2 units are positioned on opposite sides of the molecule.[27] The two PDI units are connected by 1,2-bis(2-phenylene)-ethylene bridge. When activated by MMAO-12, the (**A**)Fe_2Cl_4 and (**A**)Co_2Cl_4 complexes are more active and the (**A**)Co_2Cl_4 complexes produces polyethylene with higher molecular weight (MW) compared to mononuclear analogues. Furthermore, these complexes are thermally

Chart 1. Multinuclear Fe and Co Ethylene Polymerization Catalysts Supported by Macrocyclic Multinucleating PDI Ligands.

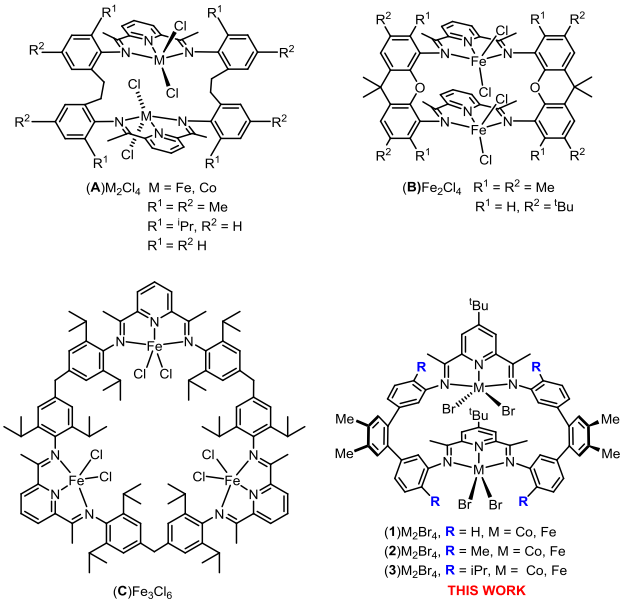

stable up to 80 ºC and display longer catalyst lifetimes than their mononuclear analogues. Takeuchi has also reported the analogous *syn*-double-decker complexes (**B**)Fe_2Cl_4, in which the PDI units are linked by 4,5-xanthene bridges and the $FeCl_2$ units are positioned on the same side of the molecule.[28] Inter-

estingly, (**B**)Fe_2Cl_4 (R^1 = R^2 = H) generates slightly branched polyethylene, with selective formation of Et and Pr branches, while the mononuclear analogue generates polyethylene with Me, Et, and Pr branches. Li has reported the trinuclear complex (**C**)Fe_3Cl_6, in which the (PDI)Fe units are linked by bis(4-phenylene)-methylene bridges. (**C**)Fe_3Cl_6 is more active, exhibits longer catalyst lifetime, and produces polyethylene with higher MW compared to the mononuclear analogue when activated by MMAO-12 or triisobutylaluminum (TIBA).[34] Based on these results, it is of interest to investigate other macrocyclic bis-PDI metal complexes in order to probe how variation of the bis-PDI ligand structure influences catalyst performance. Here we report the synthesis of a new family of macrocyclic bis-PDI ligands **1-3** and the corresponding dinuclear metal complexes (**1-3**)M_2Br_4 (M = Zn, Fe, Co), in which the PDI units are connected by a 3,3''-*ortho*-terphenyl linker (Chart 1). The ethylene homopolymerization behavior of (**1-3**)Fe_2Br_4 and (**1-3**)Co_2Br_4 is also reported.

RESULTS AND DISCUSSION

Synthesis of bis-PDI ligands. The reaction of 4-*tert*-butyl-2,6-diacetylpyridine with the appropriate dianiline under Dean-Stark imine-condensation conditions results in formation of the 30-membered macrocyclic bis-PDI ligands **1-3** in 50 – 65 % isolated yield (Scheme 1). The NMR features of **1-3** are consistent with the bis-PDI form of the ligand and indicative of highly symmetric structures, as only one set of *m*-pyridine, imine-Me, and terphenyl-Me resonances are present.

Table 1. Metal-metal Distances and Angles Between the PDI Planes (∠PDI-PDI) for (1-3)M_2Br_4 Complexes

	M-M Distance (Å)	<PDI-PDI (º)
(**1**)Zn_2Br_4	5.7600(8)	81.92
(**1**)Co_2Br_4	6.232(1)	54.09
(**1**)Co_2Br_4•$(H_2O)_{0.23}$	5.821(1)	49.08
(**2**)Zn_2Br_4	5.8668(7)	55.69
(**2**)Co_2Br_4	5.832(1)	56.12
(**3**)Fe_2Br_4	6.051(1)	57.31

Synthesis and Structures of Metal Complexes. The reaction of **1-3** with 2 equiv of MBr_2 affords the dinuclear complexes (**1-3**)M_2Br_4 in >70% isolated yield (Scheme 1). X-ray quality crystals of (**1**)Zn_2Br_4•$4(C_2H_4Cl_2)$, {(**1**)Co_2Br_4)}{(**1**)Co_2Br_4•$(H_2O)_{0.23}$}•$2(C_2H_4Cl_2)$, (**2**)Zn_2Br_4•$5(C_2H_4Cl_2)$, (**2**)Co_2Br_4•$6(C_2H_4Cl_2)$, and (**3**)Fe_2Br_4•$4(C_2H_4Cl_2)$ were grown by slow diffusion of hexanes into a 1,2-dichloroethane solution of the corresponding complex (Figures 1–5). In the solid state, all of the complexes adopt approximately C_s-symmetric angular structures in which the (PDI)M planes are skewed 49-82º relative to each other and both middle rings of the *ortho*-terphenyl bridges are on the same side of the molecule, i.e. C_s-*skew-syn* structures. The metal-metal distances for (**1-3**)M_2Br_4 are listed in Table 1 and range from 5.7600(8) to 6.232(1) Å. Similar distances were observed for macrocyclic bis-PDI complexes in which the PDI units are bridged by *m*-xylylene linkers, including ([**D**]Cu_2Im][CF_3SO_3]$_3$ (Cu-Cu = 5.9181(9) Å), [**E**]Zn_2Ox][CF_3SO_3]$_2$ (Zn-Zn = 5.3849(6) Å), (**F**)Zn_2Cl_4 (Zn-Zn = 5.515(1) Å), and (**F**)Co_2Cl_4 (Co-Co = 5.501(1) Å), which are shown in Chart 2.[35–39] In contrast, the Co-Co distance in

Scheme 1. Synthesis of Macrocyclic bis-PDI Ligands 1-3 and Their Metal Complexes (1-3)M_2Br_4 (M = Zn, Co, Fe).

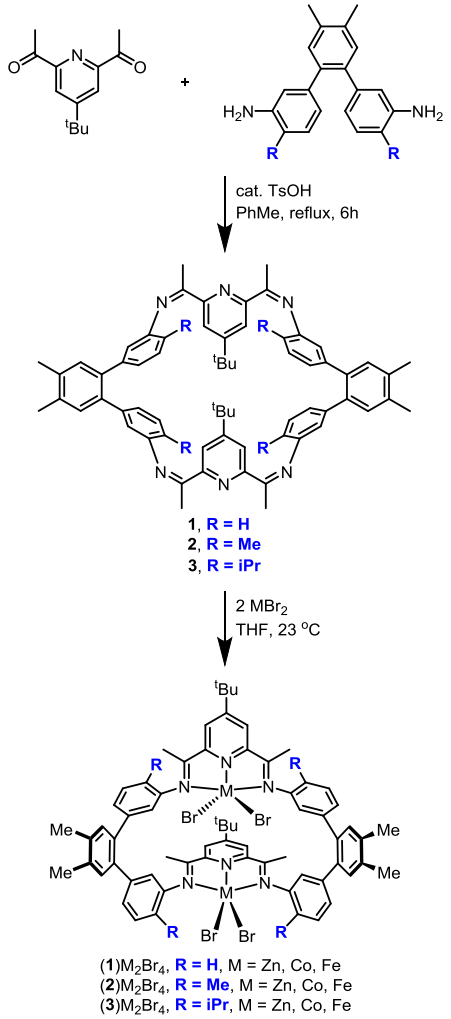

(**A**)Co_2Cl_4 (R^1 = R^2 = H; 7.731(2) Å) is much longer. While the *syn*-double-decker complexes (**B**)Fe_2Cl_4 have not been crystallographically characterized, Groysman has reported a similar [(**B**)$Co_2(CH_3CN)_4$][$Co(CO)_4$]$_2$ complex with a Co-Co distance of 4.628(1) Å.[40] The other metrical parameters for the (**1-3**)M_2Br_4 complexes are consistent with those for mononuclear (PDI)MX_2 (X = Cl, Br) complexes.[2,41] (**1**)Zn_2Br_4•$4(C_2H_4Cl_2)$ contains one distorted square-pyramidal Zn center and one trigonal-bipyramidal Zn center (Br1-Zn1-Br2 =111.27(3)º, Br3-Zn2-Br4 = 125.03(3)º). In the other four structures, the metal centers adopt distorted square pyramidal geometries with Br-M-Br angles in the range of 108 – 118º. There are two independent molecules of (**1**)Co_2Br_4 in the asymmetric unit of {(**1**)Co_2Br_4}{(**1**)Co_2Br_4•$(H_2O)_{0.23}$}•$2(C_2H_4Cl_2)$, which have similar C_s-*skew-syn* structures. One (**1**)Co_2Br_4 molecule is shown in Figure 2. The second Co site contains 23% of (**1**)Co_2Br_4•(H_2O), in which one of the Co centers has a distorted octahedral geometry with an adventitious H_2O ligand (see Supporting Information).

NMR Characterization of (1-3)M_2Br_4 Complexes. The ^{1}H NMR spectra of (**1**)Zn_2Br_4 indicate that this complex undergoes a fluxional process that permutes the two PDI units. The ^{1}H NMR and ^{1}H-^{1}H COSY spectra of (**1**)Zn_2Br_4 collected at –

Chart 2. Macrocyclic Bis-PDI Metal Complexes in which the PDI Units are Bridged by *m*-Xylylene Linkers.

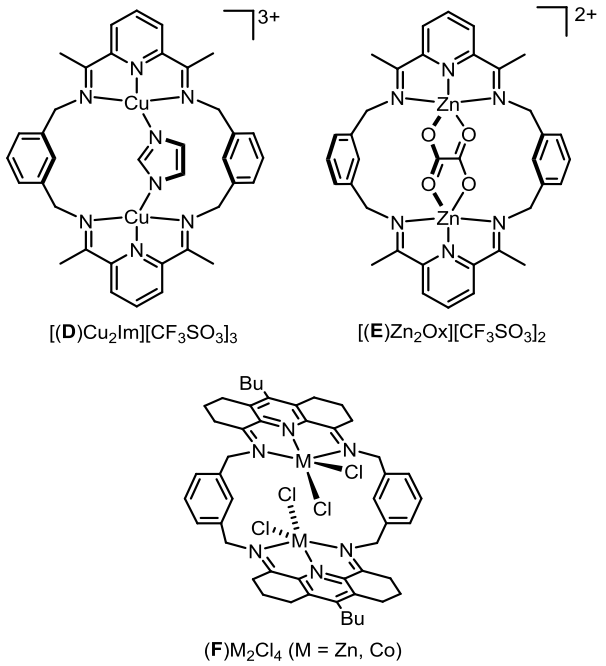

[(**D**)Cu_2Im][CF_3SO_3]$_3$ [(**E**)Zn_2Ox][CF_3SO_3]$_2$

(**F**)M_2Cl_4 (M = Zn, Co)

78 °C show the presence of two C_s-symmetric species in an ca. 2/1 ratio. Two *m*-pyridine resonances and two sets of resonances for the aromatic hydrogens of the central and lateral rings of the *ortho*-terphenyl linker in a 1/1 ratio are observed for both species (the imine-Me, terphenyl-Me and ^{t}Bu resonances for both species overlap). These isomers likely differ in the conformation of the macrocyclic bis-PDI ligand. The ^{1}H NMR spectrum at room temperature is broad. However, the ^{1}H NMR spectrum at 100 °C contains sharp singlets for the *m*-pyridine, imine-Me and terphenyl-Me hydrogens, indicative of fast exchange of the (PDI)M units and concomitant fast interconversion of the two low-temperature isomers. The paramagnetic ^{1}H NMR spectra of (**1**)Co_2Br_4 and (**2**)Fe_2Br_4 are broad and uninformative. The room temperature ^{1}H NMR spectra for the (**2**)M_2Br_4 and (**3**)M_2Br_4) complexes indicate that these complexes have C_s symmetric structures and that permutation of the two PDI units is slow on the NMR time scale. Two *m*-pyridine, imine-Me, terphenyl-Me, and ^{t}Bu resonances in an 1/1 intensity ratio are observed for (**2**)Zn_2Br_4 and (**3**)Zn_2Br_4.[42] Likewise, the paramagnetic ^{1}H NMR spectra of (**2**)M_2Br_4 and (**3**)M_2Br_4 (M = Fe, Co) are sharp and are consistent with C_s-symmetric structures.[43] These data indicate that the Me and ^{i}Pr substituents in (**2**)M_2Br_4 and (**3**)M_2Br_4 slow the fluxional process that is observed for (**1**)M_2Br_4.

Magnetic Data. Magnetic data for mononuclear (PDI)$CoCl_2$ and (PDI)$FeCl_2$ are consistent with high-spin complexes with S = 3/2 Co^{2+} and S = 2 Fe^{2+} centers respectively.[2] Due to unquenched angular moment, the experimentally determined μ_{eff} values for these complexes (4.6 - 4.9 BM for (PDI)$CoCl_2$ and 4.7 - 5.5 BM for (PDI)FeX_2 (X = Cl, Br)) are typically larger than the spin-only values ($\mu_{S.O.}$) of 3.9 BM for Co^{2+} and 4.9 for Fe^{2+}.[2,44] The $\mu_{S.O.}$value of a dinuclear metal complex with non-interacting metal centers is given by eq 1,

$$\mu_{S.O.} = 2\sqrt{S_1(S_1+1) + S_2(S_2+1)} \quad (1)$$

in which S_1 and S_2 are the spin states of the two metal centers.[45,46] The μ_{eff} values for (**1**)Co_2Br_4 and (**3**)Co_2Br_4 determined by the Evans method are 7.9(7) BM and 7.8(8) BM respectively, consistent with two independent high-spin (S_1 = S_2 = 3/2) Co^{2+} centers ($\mu_{S.O.}$ = 5.5 BM, eq 1). The μ_{eff} values for (**1**)Fe_2Br_4 and (**3**)Fe_2Br_4 determined by the Evans method are 8.4(7) BM and 8.9(5) BM respectively, consistent with two independent high-spin (S_1 = S_2 = 2) Fe^{2+} centers ($\mu_{S.O.}$ = 6.9 BM, eq 1). Complexes of **2** are poorly soluble in CD_2Cl_2, which precludes accurate determination of μ_{eff} by the Evan's method.

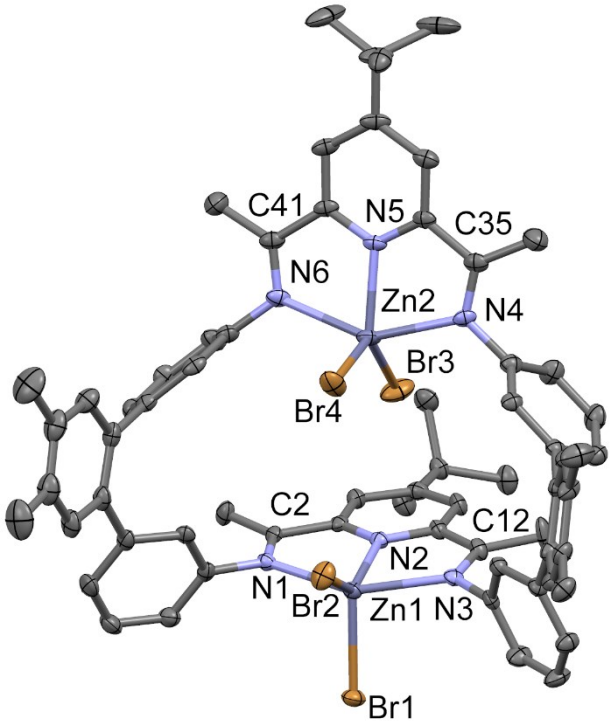

Figure 1. Solid-state structure of (**1**)Zn_2Br_4•4($C_2H_4Cl_2$). H atoms, $C_2H_4Cl_2$ molecules, and the disorder of the ^{t}Bu groups are omitted. Key bond distances (Å): C2–N1 1.287(5), C12–N3 1.280(5), N1–Zn1 2.251(3), N3–Zn1 2.254(3), N2–Zn1 2.076(3), Zn1–Br1 2.4261(7), Zn1–Br2 2.365(1), C41–N6 1.274(4), C35–N4 1.276(4), N6–Zn2 2.273(3), N4-Zn2 2.259(3), N5–Zn2 2.092(2), Zn2–Br3 2.364(1), Zn2–Br4 2.3676(8). Key bond angles (°): N1–Zn1–N3 146.6(1), N1–Zn1–N2 73.5(1), N3–Zn1–N2 73.9(1), N2–Zn1–Br1 108.94(8), N2–Zn1–Br2 139.76(8), Br1–Zn1–Br2 111.27(3), N4–Zn2–N6 146.6(1), N4–Zn2–N5 73.4(1), N6–Zn2–N5 73.4(1), N5–Zn2–Br3 124.74(9), N5–Zn2–Br4 110.18(8), Br3–Zn2–Br4 125.03(3). Color key: C gray, N light blue, Zn light gray, Br brown.

Ethylene Reactivity. The ethylene reactivity of (**1-3**)Fe_2Br_4 is summarized in Table 2. (**1**)Fe_2Br_4/1,000 TIBA reacts with ethylene to produce 1-butene with low activity (entry 1). Attempted activation of (**1**)Fe_2Br_4 with MAO or MMAO-12 in the presence of ethylene resulted in fast decomposition to Fe^0, indicating that these Al-Me reagents are able to reduce the Fe^{2+} centers.[47–49] However, (**2**)Fe_2Br_4/1,000 MMAO-12 (entry 2) and (**3**)Fe_2Br_4/1,000 MMAO-12 or TIBA (entries 3,4) produce linear polyethylenes with broad and typically bimodal molecular weight distributions (MWDs) and T_m values between 125 – 130 °C. (**3**)Fe_2Br_4/1,000 MMAO-12 is about twice as active and produces polyethylene with much higher M_w compared to (**2**)Fe_2Br_4/1,000 MMAO-12 (entries 2,3). (**3**)Fe_2Br_4/1,000 TIBA is more active than (**3**)Fe_2Br_4/1,000

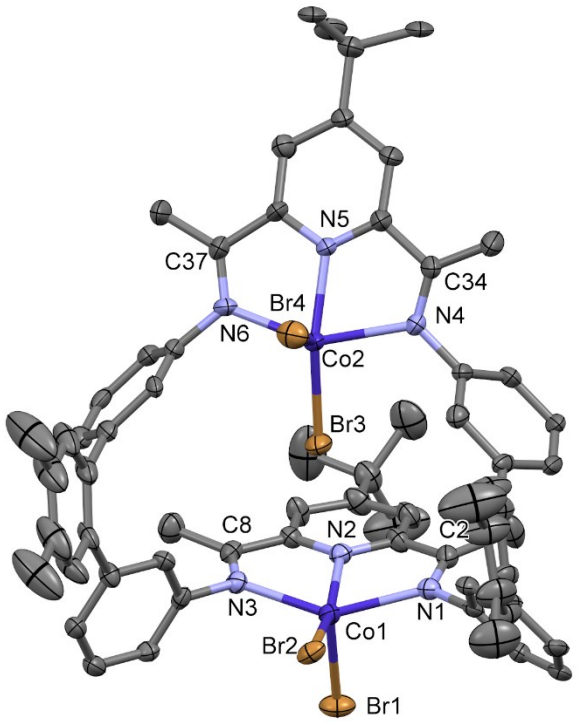

Figure 2. Structure of one (**1**)Co_2Br_4 molecule in {(**1**)Co_2Br_4}{(**1**)Co_2Br_4•$(H_2O)_{0.23}$}•2($C_2H_4Cl_2$). H atoms and $C_2H_4Cl_2$ molecules are omitted. Key bond distances (Å): C8–N3 1.284(8), C2–N1 1.281(8), N3–Co1 2.156(5), N1–Co1 2.196(5), N2–Co1 2.046(5), Co1–Br1 2.497(1), Co1–Br2 2.385(1), C37–N6 1.267(9), C34–N4 1.275(9), N6–Co2 2.181(6), N4–Co2 2.198(5), N5–Co2 2.047(5), Co2–Br3 2.401(1), Co2–Br4 2.438(1). Key bond angles (º): N3–Co1–N1 144.3(2), N3–Co1–N2 74.1(2), N1–Co1–N2 74.3(2), N2–Co1–Br1 90.8(1), N2–Co1–Br2 160.7(1), Br1–Co1–Br2 108.45(4), N6–Co2–N4 145.9(2), N6–Co2–N5 74.5(2), N5–Co2–N4 73.9(2), N5–Co2–Br3 147.3(2), N5–Co2–Br4 94.5(2), Br3–Co2–Br4 118.11(4). Color key: C gray, N light blue, Co blue, Br brown.

MMAO-12 but produces polyethylene with much lower M_w. One possible reason for the lower activity of (**3**)Fe_2Br_4/MMAO-12 vs. (**3**)Fe_2Br_4/TIBA is that access of the large linear/cyclic chains of MMAO-12 to the intermetallic cavity is hindered by steric factors.[50–53]

The broad MWDs observed for the polymers produced by (**2**)Fe_2Br_4/MMAO-12 and (**3**)Fe_2Br_4/MMAO-12 are not surprising, as similar results have been observed for mononuclear (PDI)FeX_2 complexes activated by MAO or MMAO-12.[1,2,34,47,54–58] This phenomenon is due to fast chain transfer to Al. In the initial stage of the polymerization when the Al-Me concentration is high, chain transfer to Al is fast and low-MW polymer is formed. In the later stages of the polymerization when the Al-Me concentration is low, chain transfer via β-H elimination predominates and results in the high-MW fraction. However, activation of mononuclear or multinuclear (PDI)$FeCl_2$ precatalysts with TIBA normally results in narrow MWDs as chain-transfer to Al is slow with this activator.[59,60] For example, (**C**)Fe_3Cl_6/1,000 MMAO-12 produces polyethylene with a polydispersity ($Đ$) of ca. 50, while (**C**)Fe_3Cl_6/1,200 TIBA generates polyethylene with a $Đ$ of ca. 4.[34] Surprisingly however, (**3**)Fe_2Br_4/TIBA produces polyethylene with a broad MWD, and the overall M_w value decreases as the Al/Fe ratio is increased from 500 to 10,000 (entries 7,8).

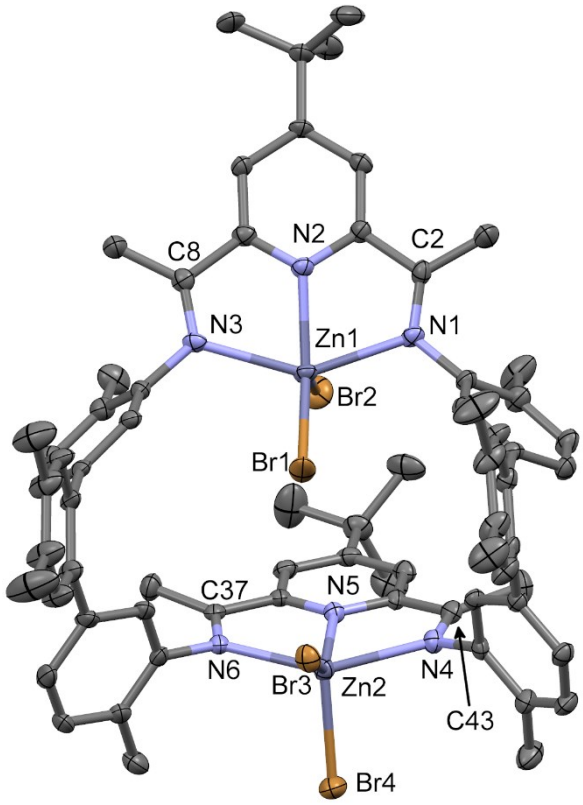

Figure 3. Structure of (**2**)Zn_2Br_4•5($C_2H_4Cl_2$). H atoms and $C_2H_4Cl_2$ molecules are omitted. Key bond distances (Å): C37–N6 1.276(6), C43–N4 1.286(6), N6–Zn2 2.248(4), N4–Zn2 2.238(3), N5–Zn2 2.081(4), Zn2–Br3 2.3694(7), Zn2–Br4 2.4216(5), C8–N3 1.262(6), C2–N1 1.277(5), N3–Zn1 2.278(4), N1–Zn1 2.289(3), N2–Zn1 2.097(3), Zn1–Br1 2.3424(8), Zn1–Br2 2.3903(7). Key bond angles (º): N6–Zn2–N4 145.0(1), N6–Zn2–N5 73.4(1), N5–Zn2–N4 73.5(1), N5–Zn2–Br3 141.9(1), N5–Zn2–Br4 107.0(1), Br3–Zn2–Br4 111.09(3), N3–Zn1–N1 142.9(1), N3–Zn1–N2 72.7(1), N2–Zn1–N1 72.6(1), N2–Zn1–Br1 141.9(1), N2–Zn1–Br2 101.4(1), Br1–Zn1–Br2 116.68(3). Color key: C gray, N light blue, Zn light gray, Br brown.

These observations indicate that chain transfer to Al occurs in these systems.

^{1}H and ^{13}C NMR analysis of the polyethylenes produced (**3**)Fe_2Br_4/1,000 MMAO-12 (Table 2, entry 3), and (**3**)Fe_2Br_4/10,000 TIBA (entry 8) confirm the operation of a chain transfer to Al pathway in these systems. In both cases the polymer is linear, >98% of the olefin units are vinyl groups and, significantly, the vinyl/saturated end group ratio is ca. 1:1.5. The excess saturated chain ends arise by chain transfer to Al. Interestingly, ^{13}C NMR analysis of the polymer produced by (**3**)Fe_2Br_4/10,000 TIBA shows that only a small fraction of saturated chain ends are ^{i}Bu ends.[58] The ^{i}Bu/^{n}Bu chain end ratio is 1/9, whereas a value of ½ is expected if the excess of saturated chain ends (not attributable to chain transfer via β-H elimination) arises by exchange of Fe-polymeryl and Al-^{i}Bu groups. Two plausible explanations for this difference are (i) Fe-*polymeryl*/Al-*H* exchange involving $^{i}Bu_2AlH$ generated by thermal decomposition of TIBA is faster than direct Fe-*polymeryl*/Al-^{i}*Bu* exchange involving TIBA,[61–65] and (ii) Fe-^{i}Bu species generated by direct Fe-*polymeryl*/Al-^{i}*Bu* exchange undergo β-H elimination to form Fe-H and isobutene prior to chain growth.

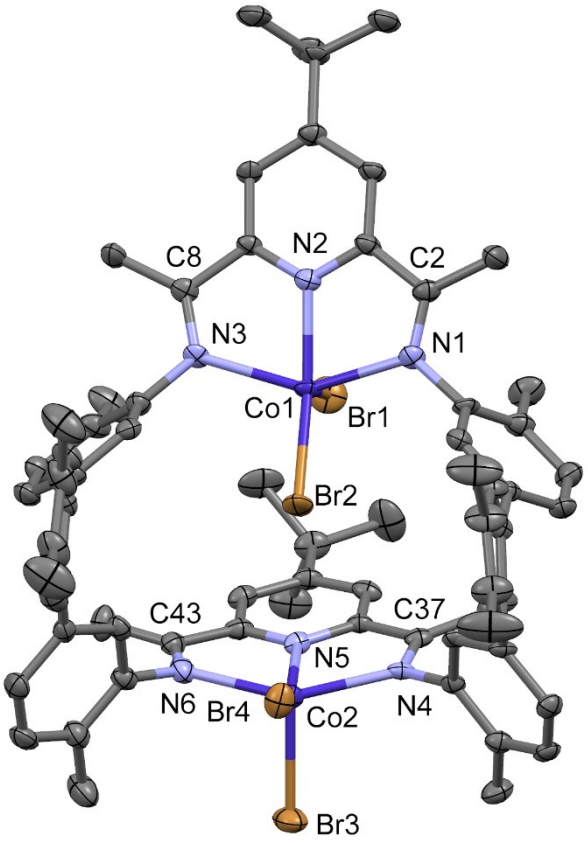

Figure 4. Structure of (**2**)Co_2Br_4•6($C_2H_4Cl_2$). H atoms and $C_2H_4Cl_2$ molecules are omitted. Key bond and atom distances (Å): C43–N6 1.280(6), C37–N4 1.285(7), N6–Co2 2.178(6), N4–Co2 2.166(6), N5–Co2 2.062(4), Co2–Br3 2.467(1), Co2–Br4 2.4044(9), C8–N3 1.290(8), C2–N1 1.277(9), N3–Co1 2.197(5), N1–Zn1 2.181(6), N2–Zn1 2.061(5), Co1–Br1 2.441(1), Co1–Br2 2.388(1). Key bond angles (º): N6–Co2–N4 146.2(2), N6–Co2–N5 74.3(2), N5–Co2–N4 74.5(2), N5–Co2–Br3 100.2(1), N5–Co2–Br4 152.4(1), Br3–Co2–Br4 107.34(4), Br1–Co1–Br2 110.30(4), N3–Co1–N1 142.3(2), N3–Co1–N2 73.7(2), N2–Co1–N1 73.6(2), N2–Co1–Br1 93.6(1), N2–Co1–Br2 156.1(1), Br1–Co1–Br2 110.30(4). Color key: C gray, N light blue, Co blue, Br brown

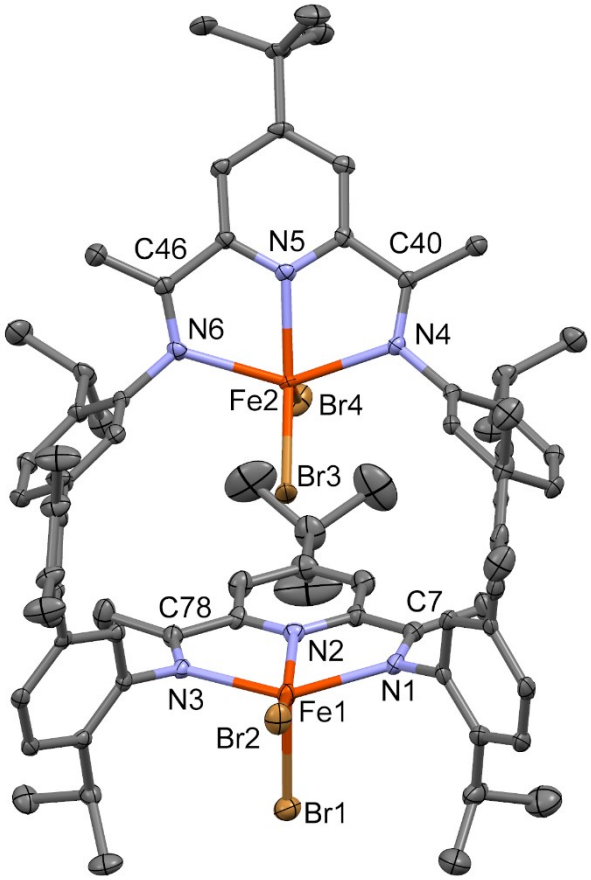

Figure 5. Structure of (**3**)Fe_2Br_4•4($C_2H_4Cl_2$). H atoms, $C_2H_4Cl_2$ molecules, and disorder of the trigonal-bipyramidal geometry of Fe2 due to H-bonding to a $C_2H_4Cl_2$ solvent mole are omitted. Key bond and atom distances (Å): C78–N3 1.272(5), C7–N1 1.280(6), N3–Fe1 2.177(4), N1–Fe1 2.190(4), N2–Fe1 2.106(3), Fe1–Br1 2.5159(8), Fe1–Br2 4168(6), C46–N6 1.276(6), C40–N4 1.274(6), N6–Fe2 2.258(4), N4–Fe2 2.289(3), N5–Fe2 2.141(4), Fe2–Br3 2.419(1), Fe2–Br4 2.4384(8). Key bond angles (º): N3–Fe1–N1 143.4(1), N3–Fe1–N2 72.9(1), N2–Fe1–N1 72.7(1), N2–Fe1–Br1 95.5(1), N2–Fe1–Br2 155.9(1), Br1–Fe1–Br2 108.53(3), Br3–Fe2–Br4 109.64(4), N6–Fe2–N4 142.8(1), N6–Fe2–N5 71.8(1), N5–Fe2–N4 72.0(1), N5–Fe2–Br3 145.1(1), N5–Fe2–Br4 105.2(1). Color key: C gray, N light blue, Fe orange, Br brown.

Attempted activation of (**1**)Co_2Br_4 and (**2**)Co_2Br_4 with MMAO-12 results in decomposition to Co^0, similar to the results for (**1**)Fe_2Br_4 noted above. Activation of (**1**)Co_2Br_4 and (**2**)Co_2Br_4 with 1,000 equiv TIBA generates catalysts that produce 1-butene with low activity (Table 2, entries 1 and 2). However, activation of (**3**)Co_2Br_4 with TIBA or MMAO-12 (Al/Co = 1000) generates catalysts that produces polyethylenes with moderate MW. (**3**)Co_2Br_4/1,000 TIBA is much less active than (**3**)Co_2Br_4/1000 MMAO-12 or (**3**)Co_2Br_4/1000 MAO but produces polyethylene with higher M_w (Table 3, entry 3).

Interestingly, in all cases, (**3**)Co_2Br_4/activator catalysts produce polyethylene with broad MWDs. ^{1}H NMR analysis of the polymer produced by (**3**)Co_2Br_4/1,000 MMAO-12 (Table 3, entry 4) shows that the vinyl/saturated end group ratio is 1/1, as expected when chain-transfer is occurring exclusively via β-H elimination. Collectively these observations imply that (**3**)Co_2Br_4/activator systems are multisite catalysts. The multisite behavior may arise in several ways. As noted above, X-ray crystallographic and NMR data show that (**3**)Co_2Br_4 adopts a C_s-symmetric structure with inequivalent metal centers, and it is possible that this feature is retained in the activated form of the catalyst. Alternatively, activation of just one of the two inequivalent metal centers may generate two distinct mono-activated species. Multisite behavior may also contribute to the broad MWDs observed when using (**2**)Fe_2Br_4 and (**3**)Fe_2Br_4.

Comparison to Literature Compounds. Chart 3 shows previously reported (PDI)MCl_2 complexes that are analogues of (**1-3**)M_2Br_4. As mononuclear (PDI)$FeBr_2$ and (PDI)$CoBr_2$ catalysts exhibit similar activity and produce polyethylene with similar MWDs to that of the corresponding (PDI)MCl_2 catalysts, it is informative to compare the behavior of (**1-3**)M_2Br_4 to that of the benchmark catalysts in Chart 3.[2,66]

Hanton reported that (**G**)$FeCl_2$/500 MMAO-3A (30% ^{i}Bu groups) oligomerizes ethylene to linear α-olefins with a Schulz-Flory propagation probability of α = 0.3 with an activi-

Table 2. Ethylene Reactivity of Dinuclear Fe Complexes.[a]

Entry	Catalyst	Activator	*T* (°C)	*P* (bar)	Activity[b] ($g_{PE}(mmol_{Fe})^{-1}h^{-1}$)	TOF (h^{-1})	M_w (Da)	$Đ^d$	T_m
1	(**1**)Fe_2Br_4	TIBA	25	2	15(5)	500	56[c] (1-butene)	–	–
2[e]	(**2**)Fe_2Br_4	MMAO-12	25	20	2,000(70)	71,000	4,500[d]	11 B	126.9
3	(**3**)Fe_2Br_4	MMAO-12	25	20	4,300(200)	150,000	280,000[d]	410 B	131.0
4[f]	(**3**)Fe_2Br_4	TIBA	25	20	9,100(30)	325,000	19,000[d]	31 B	125.1
5	(**3**)Fe_2Br_4	TIBA	60	20	5,800(400)	210,000	22,000[d]	32 B	127.1
6	(**3**)Fe_2Br_4	TIBA	80	20	6,000(600)	210,000	16,000[d]	30 B	126.2
7[g]	(**3**)Fe_2Br_4	TIBA	25	20	5,900(600)	210,000	37,000[d]	54 B	127.9
8[h]	(**3**)Fe_2Br_4	TIBA	25	20	7,800(400)	280,000	17,000[d]	95 M	124.7

[a]2.5 μmol Fe, 50 mL PhMe, 1000 equiv Al/Fe, 0.5 h; [b]average of two runs, number in parentheses is the standard deviation for those runs; [c]determined by GC-MS; [d]determined by GPC, M = monomodal molecular weight distribution, B = bimodal molecular weight distribution; [e]C_6-C_{28} α-olefins also observed, α = 0.86; [f]exotherm to 80 °C observed upon activation in this case; [g]500 equiv Al/Fe; [h]0.25 μmol Fe, 10,000 equiv Al/Fe.

Table 3. Ethylene Reactivity of Dinuclear Co Complexes.[a]

Entry	Catalyst	Activator	*T* (°C)	*P* (bar)	Activity[b] ($g_{PE}(mmol_{Co})^{-1}h^{-1}$)	TOF (h^{-1})	M_w (Da)	$Đ^d$	T_m
1	(**1**)Co_2Br_4	TIBA	25	2	15(5)	500	56[c] (1-butene)	–	–
2	(**2**)Co_2Br_4	TIBA	25	2	30(5)	1,000	56[c] (1-butene)	–	–
3	(**3**)Co_2Br_4	TIBA	25	20	19(4)	680	180,000[d]	140 B	130.6
4	(**3**)Co_2Br_4	MMAO-12	25	20	260(20)	9,300	82,000[d]	220 M	126.5
5	(**3**)Co_2Br_4	MAO	25	20	250(10)	8,900	76,000[d]	83 M	126.8

[a]2.5 μmol Co, 50 mL PhMe, 1000 equiv Al/Co, 0.5 h; [b]average of two runs, number in parentheses is the standard deviation of those runs; [c]determined by GC-MS; [d]determined by GPC; M = monomodal molecular weight distribution, B = bimodal molecular weight distribution.

ty of 1,625 $(g_{PE})(mmol_{Co}^{-1})h^{-1}$, and (**G**)$CoCl_2$/500 MMAO-3A dimerizes ethylene to >99% 1-butene with an activity of 3,000 $(g_{PE})(mmol_{Co}^{-1})h^{-1}$.[67] In contrast, both (**1**)Fe_2Br_4/1,000 TIBA and (**1**)Co_2Br_4/1,000 TIBA produce 1-butene selectivity but with much lower activity. However, the activity of (PDI)MCl_2 catalysts generally varies with the activator in the order: MAO > MMAOs > TIBA, and thus the lower activity of the (**1**)M_2Br_4 catalysts may in part reflect the difference in activator.[59,60]

Gibson and Brookhart reported that (**H**)$FeCl_2$/500 MMAO-3A and (**H**)$FeCl_2$/1,000 MAO generate linear α-olefins (α = 0.8) with a turnover frequency (TOF) of 1 x 10^5 h^{-1}.[68] The dinuclear analogue (**2**)Fe_2Br_4/MMAO-12 exhibits a similar TOF of 0.7 x 10^5 h^{-1} but produces an insoluble polyethylene fraction. (**H**)$CoCl_2$/1,000 MAO also generates linear α-olefins (α = 0.65) but with low activity (25 $g/mmol_{Co}^{-1}$ h^{-1}).[44] Similar activity is observed with (**2**)Co_2Br_4/1,000 TIBA, but 1-butene is selectively generated.

(**I**)$FeCl_2$/500 MMAO-3A generates linear α-olefins (α = 0.8-0.9) with a TOF of ca. 8 x 10^4 h^{-1}.[68] In contrast, (**3**)Fe_2Br_4/1,000 MMAO-12 and (**3**)Fe_2Br_4/1,000 TIBA are 3-4 times more active and produce solid polyethylene products. The geometric constraints and additional steric crowding imparted by the dinuclear structure of (**3**)Fe_2Br_4 may contribute to this difference. The ethylene homopolymerization behavior of (**I**)$CoCl_2$ has not been reported.

Chart 3. Mononuclear Analogs for (1-3)M_2Br_4 (M = Co, Fe).

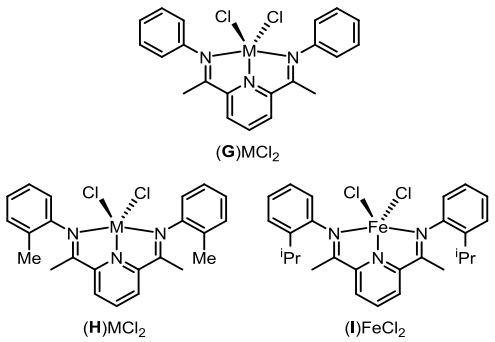

(**2**)Fe_2Br_4/1,000 MMAO-12 is a ca. five times more active than (**B**)Fe_2Cl_4/1,000 MMAO-12 (R^1 = R^2 = Me, activity 356 $g_{PE}(mmol_{Fe1})^{-1}$ h^{-1} at 25 °C) but produces polyethylene with a lower M_w (4,500 Da vs 75,500 Da). (**3**)Fe_2Br_4/1,000 MMAO-12 is ca. six times more active than (**A**)Fe_2Cl_4/1,000 MMAO-12 (R^1 = ^{i}Pr, R^2 = H, activity = 684 $g_{PE}(mmol_{Fe})^{-1}$ h^{-1} at 25 °C)

and produces polymer with a higher MW M_w = 280,000 vs. 100,000 Da).

EXPERIMENTAL SECTION

General Procedures. All experiments were performed using dry-box or Schlenk techniques under a nitrogen atmosphere unless noted otherwise. Nitrogen was purified by passage through Q-5 oxygen scavenger and activated molecular sieves. CH_2Cl_2, Et_2O, THF were dried by passage through activated alumina. Hexanes and toluene were purified by passage through BASF R3−11 oxygen scavenger and activated alumina. CH_2ClCH_2Cl was dried over $MgSO_4$ and then distilled from calcium hydride and stored under nitrogen. $CDCl_3$, CD_2Cl_2, $CDCl_2CDCl_2$ were distilled from and stored over activated 3 Å molecular sieves. Anhydrous metal salts, $(PPh_3)_4Pd$, and $PdCl_2$(dppf) were purchased from Strem Chemical, Inc. and used without further purification. 5-bromo-2-methyl aniline, 3-aminophenylboronic acid pinacol ester, 2,5-dibromo-*o*-xylene, and B_2pin_2 were purchased from AK Scientific and used without further purification. Anhydrous dioxane, TIBA, MAO, and MMAO-12 (5% ^{n}Bu groups) were purchased from MilliporeSigma. 2-nitrocumene purchased from TCI America. 4-*tert*-butyl-2,6-diacetylpyridine was synthesized according to literature procedures.[69] 5-bromo-2-isopropyl-aniline was synthesized from 2-nitrocumene using literature procedures for 5-bromo-2,6-dimethylaniline.[70]

NMR spectra were recorded on Bruker ADVANCE II+ 500 or DRX 400 spectrometers at room temperature unless otherwise specified. ^{1}H and ^{13}C chemical shifts are reported relative to $SiMe_4$ and internally referenced to residual ^{1}H and ^{13}C solvent resonances. The baselines of the ^{1}H NMR spectra for the paramagnetic compounds were spline corrected. Peak integrations for the spectra of the paramagnetic compounds were unreliable and only δ and $\upsilon_{1/2}$ values for the resonances are reported.

MALDI-TOF-TOF-MS spectra were collected on a Bruker Ultraflextreme instrument using dithranol as the matrix. High-resolution accurate mass spectra (HRA-MS) were recorded on an Agilent 6224 TOF−MS instrument in mixed (ESI/APCI) mode. While the expected $[M-Br]^+$ ion was observed by MALDI-TOF-TOF-MS for all metal complexes, ions of the form $[M-xBr+yCl]^+$ were instead observed by by HRA-MS, with $[M-4Br+3Cl]^+$ being the most prevalent. We attribute this phenomenon to formation of Cl^- ions during ionization, originating from the CH_2Cl_2 solvent used for analysis. The observed isotope patterns closely matched isotope patterns calculated using envipat 2.2 Web and are reported in the SI for each metal complex.[71] The reported *m*/*z* value corresponds to the most intense peak in the isotope pattern. X-ray quality crystals of (**1**)Zn_2Br_4•4($C_2H_4Cl_2$), {(**1**)Co_2Br_4}{(**1**)Co_2Br_4•($H_2O)_{0.23}$}•2($C_2H_4Cl_2$), (**2**)Zn_2Br_4•5($C_2H_4Cl_2$), (**2**)Co_2Br_4•6($C_2H_4Cl_2$), and (**3**)Fe_2Br_4•4($C_2H_4Cl_2$) were grown by diffusion of hexanes into a 1,2-dichloroethane solution (1/1) of each compound at room temperature over 2 d. Thermal ellipsoids are drawn at the 50% probability level.

Elemental analyses were performed by Midwest Microlab. In most cases the ligands and metal complexes did not combust well and significant deviations in C% (3-5%) but accurate H% and N% values (typically within ±0.4%) were observed. The elemental analysis results are included for completeness.

3-Amino-4-methylphenylboronic acid pinacol ester (Scheme 2). 5-Bromo-2-methylaniline (6.49 g, 34.9 mmol, 1 equiv), B_2pin_2 (9.74 g, 38.4 mmol, 1.1 equiv), $PdCl_2$(dppf) (684 mg, 1 mmol, 3 mol%), and KOAc (14.8, 105 mmol, 3 equiv) were added to a side-armed round bottom flask under an N_2 purge. Dioxane (90 mL) was added by syringe. A condenser was attached and the reaction mixture was refluxed for 3 h. The reaction mixture was cooled to room temperature and the solvent was removed under vacuum. The crude black solid was dissolved in EtOAc/CH_2Cl_2 (1/9), filtered through Celite, and chromatographed on silica gel to yield 3-amino-4-methylphenylboronic acid pinacol ester as a white solid. Yield: 4.16 g, 51.1 %.^{1}H NMR: ($CDCl_3$, 400 MHz): δ 7.16 (d, $^3J_{HH}$ = 7.4 Hz, 1H, Ar-H^5), 7.12 (s, 1H, Ar-H^2), 7.07 (d, $^3J_{HH}$ = 7.2 Hz, 1H, Ar-H^6), 3.57 (s, 2H, -NH_2), 2.18 (s, 3H, Ar-CH_3), 1.33 (s, 12H, B-O-C-(CH_3)$_2$). ^{13}C{^{1}H} NMR: ($CDCl_3$, 100 MHz): δ 144.2, 130.1, 126.0, 125.4, 121.2, 83.7 (B-O-*C*-(CH_3)$_2$), 25.0 (B-O-C-(*C*H_3)$_2$), 17.7 (Ar-*C*H_3); the B-*C* resonance was not observed. ESI/APCI-TOF HRA-MS (m/z): $[M+H]^+$ Calcd for $C_{13}H_{21}BNO_2^+$ 234.1660; Found 234.1667.

3-Amino-4-isopropylphenylboronic acid pinacol ester (Scheme 2). This compound was synthesized by the procedure for 3-amino-4-methylphenylboronic acid pinacol ester using 5-bromo-2-isopropyl-aniline (3.50 g, 16.4 mmol, 1 equiv), B_2pin_2 (4.57 g, 18.0 mmol, 1.1 equiv), $PdCl_2$(dppf) (401 mg, 0.49 mmol, 3 mol%), and KOAc (4.81 g, 49.0 mmol, 3 equiv). The crude product was chromatographed on silica gel using EtOAc/CH_2Cl_2 (0.5/9) to yield 3-amino-4-isopropylphenylboronic acid pinacol ester as a white solid. Yield: 2.89 g, 67.0 %. ^{1}H NMR ($CDCl_3$, 400 MHz): δ 7.25 (dd, $^3J_{HH}$ = 9.5 Hz, $^4J_{HH}$ = 1.3 Hz, 1H, Ar-H^6, overlapped with solvent resonance), 7.17 (d, $^3J_{HH}$ = 9.5 Hz, 1H, Ar-H^5), 7.14 (d, $^3J_{HH}$ = 1.3 Hz, Ar-H^2), 3.64 (s, 2H, -NH_2), 2.92 (sept, $^3J_{HH}$ = 6.9 Hz, 1H, Ar-C*H*(CH_3)$_2$), 1.33 (s, 12H, B-O-C-(CH_3)$_2$), 1.26 (d, $^3J_{HH}$ = 6.8 Hz, 6H, Ar-CH(CH_3)$_2$). ^{13}C{^{1}H} NMR ($CDCl_3$, 100 MHz): δ 142.9, 136.3, 125.7, 125.0, 122.2, 83.7 (B-O-*C*-(CH_3)$_2$), 27.9 (Ar-*C*H(CH_3)$_2$, 25.0 (B-O-C-(*C*H_3)$_2$), 22.3 (Ar-CH(*C*H_3)$_2$); the B-*C* resonance was not observed. ESI/APCI-TOF HRA-MS (m/z): $[M+H]^+$ Calcd for $C_{15}H_{25}BNO_2^+$ 262.1973; Found 262.1977.

Scheme 2. Synthesis of 3-Amino-4-R-phenylboronic Acid Pinacol Esters (R = Me, ^{i}Pr)

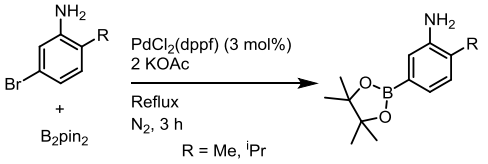

4',5'-Dimethyl-[1,1':2',1''-terphenyl]-3,3''-diamine (Scheme 3). 2,5-Dibromo-*o*-xylene (2.79 g, 10.5 mmol, 1 equiv), 3-aminophenylboronic acid pinacol ester (4.83 g, 22.1 mmol, 2.1 equiv), $Pd(PPh_3)_4$ (345 mg, 0.30 mmol, 3 mol%), and K_2CO_3 (5.80 g, 42.0 mmol, 4 equiv) were added to a side-armed round bottom flask under N_2. Dioxane (25 mL) and degassed H_2O (25 mL) were added by syringe. A condenser was attached, and the reaction mixture was refluxed for 16 h. The mixture was cooled to room temperature and the dioxane was removed under vacuum, yielding a slurry of a yellow solid in a colorless supernatant. CH_2Cl_2 (25 mL) was added and the biphasic mixture was stirred until the solid dissolved. The aqueous layer was extracted with CH_2Cl_2 (2 x 25 mL) and the combined organic layers were washed with saturated aqueous $NaHCO_3$ (3 x 15 mL), dried with $MgSO_4$ and filtered. The solvent was removed under vacuum. The crude red oil was dissolved in EtOAc/hexanes (3/1) and chromatographed on silica gel to yield 4',5'-dimethyl-[1,1':2',1''-terphenyl]-3,3''-diamine as a white solid. Yield: 2.51 g, 83.0 %. ^{1}H NMR ($CDCl_3$, 500 MHz): δ 7.19 (s, 2H, H_e), 6.98 (t, $^3J_{HH}$ = 7.9 Hz, 2H, H_c), 6.53 (m, 6H, H_a, H_b, H_d), 3.54 (s, 4H, -NH_2), 2.33 (s, 6H, terphenyl-CH_3). ^{13}C{^{1}H} NMR ($CDCl_3$, 126 MHz): δ 145.9, 142.9, 138.2, 135.7, 131.9, 128.7, 120.8, 116.8, 113.3, 19.5 (terphenyl-*C*H_3). ESI/APCI-TOF HRA-MS (m/z): $[M+H]^+$ Calcd for $C_{20}H_{21}N_2^+$ 289.1699; Found 289.1706.

4,4',4'',5'-Tetramethyl-[1,1':2',1''-terphenyl]-3,3''-diamine (Scheme 3). This compound was synthesized by the procedure for 4',5'-dimethyl-[1,1':2',1''-terphenyl]-3,3''-diamine using 2,5-dibromo-*o*-xylene (2.49 g, 9.43 mmol, 1 equiv), 3-amino-4-methylphenylboronic acid pinacol ester (4.50 g, 19.3 mmol, 2.1 equiv), $Pd(PPh_3)_4$ (327 mg, 0.28 mmol, 3 mol%), and K_2CO_3 (5.02 g, 36.3 mmol, 4 equiv). The crude red oil was dissolved in EtOAc/hexanes (1/1) and chromatographed on silica gel to yield 4,4',4'',5'-tetramethyl-[1,1':2',1''-terphenyl]-3,3''-diamine as a white solid. Yield: 2.11 g, 71.0 %. ^{1}H NMR ($CDCl_3$, 500 MHz): δ 7.10 (s, 2H, H_e), 6.86 (d, $^3J_{HH}$ = 7.6 Hz, 2H, H_c), 6.51 (d, $^3J_{HH}$ = 1.6 Hz, 2H, H_a), 6.43 (dd, $^3J_{HH}$ = 7.6 Hz, $^4J_{HH}$ = 1.7 Hz, 2H, H_d), 3.54 (s, 4H, -NH_2), 2.30 (s, 6H, H_b), 2.11 (s, 6H, terphenyl-CH_3). ^{13}C{^{1}H} NMR ($CDCl_3$, 126 MHz): δ 144.7, 141.1, 138.3, 135.7, 132.1, 130.0, 120.6, 120.6, 116.4, 19.4 (terphenyl-CH_3), 17.2 (*C*-H_b). ESI/APCI-TOF

HRA-MS (m/z): $[M+H]^+$ Calcd for $C_{22}H_{24}N_2^+$ 317.2012; Found 317.2006.

4,4''-Diisopropyl-4',5'-tetramethyl-[1,1':2',1''-terphenyl]-3,3''-diamine (Scheme 3). This compound was synthesized by the procedure for 4',5'-dimethyl-[1,1':2',1"-terphenyl]-3,3"-diamine using 2,5-dibromo-*o*-xylene (2.90 g, 11.0 mmol, 1 equiv), 3-amino-4-isopropylphenylboronic acid pinacol ester (6.0 g, 23.0 mmol, 2.1 equiv), $Pd(PPh_3)_4$ (379 mg, 0.33 mmol, 3 mol%), and K_2CO_3 (6.04 g, 43.7 mmol, 4 equiv). The crude red oil was dissolved in EtOAc/Hex (3/7) and chromatographed on silica gel to yield 4,4''-diisopropyl-4',5'-tetramethyl-[1,1':2',1''-terphenyl]-3,3''-diamine as a pale yellow solid. Yield: 3.13 g, 76.5 %. ^{1}H NMR ($CDCl_3$, 500 MHz): δ 7.12 (s, 2H, H_d), 6.96 (d, $^3J_{HH}$ = 7.8 Hz, 2H, H_b), 6.51 (m, 4H, H_a and H_c), 3.58 (s, 4H, -NH_2), 2.86 (sept, $^3J_{HH}$ = 6.8 Hz, 2H, Ar-CH(CH$_3$)$_2$), 2.30 (s, 6H, terphenyl-CH_3), 1.22 (d, $^3J_{HH}$ = 6.8 Hz, 12H, Ar-CH(CH_3)$_2$). ^{13}C{^{1}H} NMR ($CDCl_3$, 126 MHz): δ 143.5, 140.6, 138.2, 135.7, 132.2, 131.0, 125.0, 120.8, 117.3, 27.8 (Ar-CH(CH$_3$)$_2$), 22.4 (Ar-CH(CH_3)$_2$), 19.4 (terphenyl-CH_3). ESI/APCI-TOF HRA-MS (m/z): $[M+H]^+$ Calcd for $C_{26}H_{33}N_2^+$ 373.2638; Found 373.2633.

Scheme 3. Synthesis and Atom Labelling Scheme of 4,4''-R$_2$-4',5'-dimethyl-[1,1':2',1''-terphenyl]-3,3''-diamines (R = H, Me ,^{i}Pr).

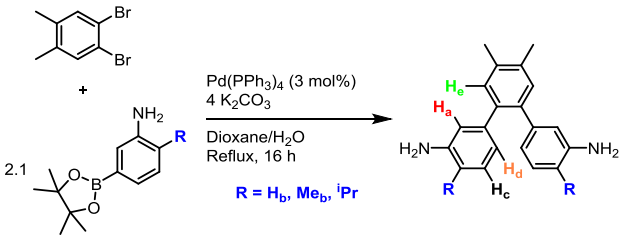

1. 4-tert-butyl-2,6-diacetylpyridine (701 mg, 3.20 mmol, 1 equiv), 4',5'-dimethyl-[1,1':2',1"-terphenyl]-3,3"-diamine (924 mg, 3.20 mmol, 1 equiv), *p*-TsOH (120 mg, 10 mol%), and PhMe (40 mL) were added to a round bottom flask. A Dean-Stark trap and condenser were attached, and the reaction mixture was refluxed for 6 h. The mixture was allowed to cool to room temperature and the PhMe was removed under vacuum. MeOH (25 mL) was added to the flask and the brown suspension was stirred for 5 min. The beige solid was collected on a sintered glass frit and washed with MeOH (2 x 20 mL) and Et_2O (2 x 5 mL) to yield **1** as a white solid. Yield 982 mg, 65.0 %. The labelling scheme for **1** is shown in Figure 6. ^{1}H NMR (CD_2Cl_2, 500 MHz): δ 8.28 (s, 4H, *m*-py), 7.29 (t, $^3J_{HH}$ = 7.7 Hz, 4H, H_c), 7.27 (s, 4H, H_e), 6.94 (d, $^3J_{HH}$ = 7.7 Hz, 4H, H_d), 6.68 (d, $^3J_{HH}$ = 7.7 Hz, 4H, H_b), 6.56 (s, 4H, H_a), 2.34 (s, 12H, terphenyl-CH_3), 2.06 (s, 12H, N=C-CH_3), 1.37 (s, 18H, ^{t}Bu). ^{13}C{^{1}H} NMR (CD_2Cl_2, 126 MHz): δ 168.2 (N=*C*), 161.2 (*p*-py), 155.5 (*o*-py), 151.8 (*C*-N=C), 143.2 (*C*$_{terphenyl}$-C$_{aniline}$), 138.5 (C$_{terphenyl}$-*C*$_{aniline}$), 136.2 (terphenyl *C*-CH$_3$), 131.9 (*C*-H_e), 129.1 (*C*-H_c), 125.1 (*C*-H_d), 121.0 (*C*-H_a), 119.4 (*m*-py), 117.5 (*C*-H_b), 35.6 (-*C*(CH$_3$)$_3$), 30.8 (-C(*C*H$_3$)$_3$), 19.5 (terphenyl-*C*H$_3$), 16.7 (N=C-*C*H$_3$).MALDI-TOF-TOF (Dithranol) (m/z): $[M+H]^+$ Calcd for $C_{66}H_{67}N_6^+$: 943.54, Found 943.36. ESI/APCI-TOF HRA-MS (m/z): $[M+H]^+$ Calcd for $C_{66}H_{67}N_6^+$ 943.5422, Found 943.5418. Anal. Calcd for $C_{66}H_{66}N_6$: C, 84.04; H, 7.05; N, 8.91. Found: C, 81.89; H, 6.99; N, 8.56.

2. This compound was synthesized by the procedure for **1** using 4-tert-butyl-2,6-diacetylpyridine (701.0 mg, 3.20 mmol, 1 equiv), 4,4',4'',5'-tetramethyl-[1,1':2',1"-terphenyl]-3,3"-diamine (1.01 g, 3.20 mmol, 1 equiv), *p*-TsOH (120 mg, 10 mol%), and PhMe (40 mL). The crude solid was washed with MeOH (20 mL) and hexanes (10 mL) to yield **2** as a white solid. Yield 840 mg, 52.5 %. The labelling scheme for **2** is shown in Figure 6. ^{1}H NMR (CD_2Cl_2, 500 MHz): δ 8.36 (s, 4H, *m*-py-H), 7.19 (s, 4H, H_e), 7.15 (d, $^3J_{HH}$ = 7.7 Hz, 4H, H_d), 6.86 (d, $^3J_{HH}$ = 7.7 Hz, 4H, H_c), 6.44 (s, 4H, H_a), 2.32 (s, 12H, terphenyl-CH_3), 2.06 (s, 12H, Me$_b$), 1.98 (s, 12H, N=C-CH_3), 1.37 (s, 18H, ^{t}Bu).^{13}C{^{1}H} NMR (CD_2Cl_2, 126 MHz): δ 167.6 (N=*C*), 161.1 (*p*-py), 155.3 (*o*-py), 150.3 (*C*-N=C), 140.8 (*C*$_{terphenyl}$-C$_{aniline}$), 138.5 (C$_{terphenyl}$-*C*$_{aniline}$), 135.9 (terphenyl *C*-CH$_3$), 131.9 (*C*-H_e), 130.4 (*C*-H_d), 125.3 (*C*-C(H_b)$_3$), 124.9 (*C*-H_c), 120.2 (*C*-H_a), 119.3 (*m*-py), 35.5 (-*C*(CH$_3$)$_3$), 30.8 (-C(*C*H$_3$)$_3$), 19.5 (terphenyl-*C*H$_3$), 17.5 (*C*-Me$_b$), 16.7 (N=C-*C*H$_3$). MALDI-TOF-TOF (Dithranol) (m/z): $[M+H]^+$ Calcd for $C_{70}H_{75}N_6$ 999.61, Found 999.61. ESI/APCI-TOF HRA-MS (m/z): $[M+H]^+$ Calcd for $C_{70}H_{75}N_6^+$ 999.6048, Found 999.6041. Anal. Calcd for $C_{70}H_{74}N_6$: C, 84.13; H, 7.46; N, 8.41. Found: C, 83.99; H, 7.66; N, 8.21.

3. This compound was synthesized by the procedure for **1** using 4-tert-butyl-2,6-diacetylpyridine (701.0 mg, 3.20 mmol, 1 equiv), 4,4''-diisopropyl-4',5''-tetramethyl-[1,1':2',1''-terphenyl]-3,3''-diamine (1.19 g, 3.20 mmol, 1 equiv), *p*-TsOH (120 mg, 10 mol%), and PhMe (40 mL). The crude solid was washed with MeOH (2 x 10 mL) and hexanes (10 mL) to yield **3** as a yellow solid. Yield 840 mg, 52.5 %. The labelling scheme for **3** is shown in Figure 6. ^{1}H NMR (CD_2Cl_2, 500 MHz): δ 8.32 (s, 4H, *m*-py), 7.23 (d, $^3J_{HH}$ = 7.9 Hz, 4H, H_c), 7.19 (s, 4H, H_e), 6.93 (dd, $^3J_{HH}$ = 7.9 Hz, $^4J_{HH}$ = 1.3 Hz, 4H, H_d), 6.45 (d, $^3J_{HH}$ = 1.3 Hz, 4H, H_a), 2.92 (sept, $^3J_{HH}$ = 6.9 Hz, 4H, -CH(CH$_3$)$_2$), 2.31 (s, 12H, terphenyl-CH_3), 2.04 (s, 12H, N=C-CH_3), 1.36 (s, 18H, ^{t}Bu), 1.15 (d, $^3J_{HH}$ = 6.8 Hz, 24H, -CH(CH_3)$_2$). ^{13}C{^{1}H} NMR (CD_2Cl_2, 126 MHz): δ 167.3 (N=*C*), 161.4 (*p*-py), 155.7 (*o*-py), 149.1 (*C*-N=C), 140.4 (*C*$_{terphenyl}$-C$_{aniline}$), 138.4 (C$_{terphenyl}$-*C*$_{aniline}$), 136.5 (*C*-CH(CH$_3$)$_2$), 135.9 (terphenyl *C*-CH$_3$), 132.1 (*C*-H_d), 125.7 (*C*-H_b), 125.5 (C-H_c), 120.2 (*C*-H_a), 119.3 (*m*-py), 35.4 (-*C*(CH$_3$)$_3$), 30.8 (-C(*C*H$_3$)$_3$), 28.7 (-*C*H(CH$_3$)$_2$), 22.9 (-CH(*C*H$_3$)$_2$), 19.5 (terphenyl-*C*H$_3$), 16.9 (N=C-*C*H$_3$). MALDI-TOF-TOF (Dithranol) (m/z): $[M+H]^+$ Calcd for $C_{70}H_{75}N_6^+$ 1111.73, Found 1111.73. ESI/APCI-TOF HRA-MS (m/z): Calcd for $C_{70}H_{75}N_6^+$ $[M+H]^+$ 1111.7300, Found 1111.7303. Anal. Calcd for $C_{78}H_{90}N_6$: C, 84.28; H, 8.16; N, 7.56. Found: C, 81.84; H, 8.10; N, 7.30.

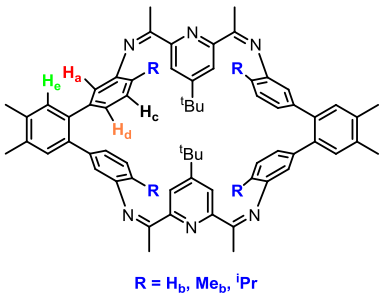

Figure 6. Atom Labelling Scheme for **1-3**.

(1)Zn$_2$Br$_4$. A vial was charged with $ZnBr_2$ (67.6 mg, 0.106 mmol, 2 equiv) and THF (5 mL). The suspension was stirred for ca. 5 min, resulting in a pale-yellow solution. **1** (50.0 mg, 0.053 mmol, 1 equiv) was added in one portion. The pale-yellow suspension was stirred for 16 h at room temperature. The solvent was removed under vacuum, and the solid was suspended in Et_2O (10 mL). The solid was collected on a glass frit and washed with Et_2O (2 x 5 mL) and hexanes (5 mL). The solid was dried under vacuum for 2 d at 100 °C to yield (**1**)Zn_2Br_4 as a pale-yellow solid. Yield: 65.4 mg, 88.6 %. The atom labelling schemes for (**1**)Zn_2Br_4 for fast and slow PDI exchange are shown in Figures 7 and 8, respectively. ^{1}H NMR (CD_2Cl_2, 500 MHz, room temperature, intermediate PDI exchange): δ 8.07 (br s, 4H, *m*-py), 7.23 (br s, 16H, H_b, H_c, H_d), 6.65 (br s, 4H, H_a), 2.31 (br s, 24H, N=C-CH_3, H_e), 1.46 and 1.33 (two br s, total integral 18H, -C(CH_3)$_3$). ^{1}H NMR (CD_2Cl_2, 500 MHz, -78 °C, slow PDI exchange) major isomer: δ 8.09 (s, 2H, H_f), 7.83 (s, 2H, H_f'), 7.77 (s, 2H, H_a), 7.41 (d, J = 7.2 Hz, H_c), 7.37 (s, 2H, H_e), 7.34 (d, J = 7.1 Hz, H_d), 7.03 (s, 2H, H_e'), 6.96 (t, ^3J = 7.3 Hz, H_c'), 6.60 (d, ^3J = 7.5 Hz, 2H, H_b'), 6.56, ^3J = 6.8 Hz, 2H, H_b), 6.48 (d, ^3J = 7.3 Hz, H_d'), 6.42 (s, 2H, H_a'); minor isomer: δ 8.15 (s, 2H, H_f), 7.97 (s, 2H, H_f'), 7.77 (s, 2H, H_a, coincident with major isomer), 7.29 (s, 2H, H_e'), 7.13 (s, 2H, H_e'), 6.32 (s, 2H, H_a'). By COSY, the rest of the aromatic resonances for the minor isomer overlap with those of the major isomer at δ 7.77, 7.41, 6.96, 6.60. The terphenyl-Me, imine-Me, and ^{t}Bu resonances for the major and minor isomers are overlapped: δ 2.54 (s, 6H), 2.52 (s, 3H), 2.39 (s, 14H), 2.20 (s, 8H), 2.00 (s, 6H), 1.38 (s, 14H, ^{t}Bu), 1.34 (s, 5H, ^{t}Bu), 1.31

(s, 11H, ^{t}Bu). ^{1}H NMR ($C_2D_2Cl_4$, 400 MHz, 100 °C, fast PDI exchange): δ 8.09 (s, 4H, *m*-py), 7.25 and 7.00 (overlapping br s, total integral 20 H, H_a, H_b, H_c. H_d, and H_e), 2.37 (br s, 12 H, H_e), 2.33 (br s, 12H, N=C-CH_3), 1.54 (s, total integral 18H, -C(CH_3)$_3$). ^{13}C{^{1}H} NMR (CD_2Cl_2, 126 MHz): δ 163.7 (br s, N=C-*C*H$_3$). 148.7 (br s), 146.9 (br s), 142.5 (br s), 137.8 (br s), 137.3 (br s), 136.7 (br s), 132.2 (br s, *C*-H_e), 128.9 (br s, *C*-H_b, *C*-H_c, or *C*-H_d), 128.1 (br s, *C*-H_b, *C*-H_c, or *C*-H_d), 127.2 (br s, *C*-H_b, *C*-H_c, or *C*-H_d), 125.5 (br s), 124.0 (br s, *m*-py), 123.6 (br s, *m*-py), 118.9 (br s, *C*-H_a), 36.6 (br s, (-*C*(CH$_3$)$_3$), 30.6 (-C(*C*H$_3$)$_3$), 19.6 (tephenyl-*C*H$_3$), 17.8 (N=C-*C*H$_3$). A total of 16 ^{13}C resonances are expected for (**1**)Zn_2Br_4 assuming fast exchange. A total of 19 are observed, which is due to the slower NMR timescale of ^{13}C versus ^{1}H. MALDI-TOF-TOF (Dithranol) (m/z): [M-Br]$^+$ Calcd for $C_{66}H_{66}N_6Zn_2Br_3^+$ 1313.14, Found 1313.14. ESI/APCI-TOF HRA-MS (m/z): [M-4Br+3Cl]$^+$ Calcd for $C_{66}H_{66}N_6Zn_2Cl_3^+$ 1179.2956, Found 1179.2981; [M-3Br+2Cl]$^+$ Calcd for $C_{66}H_{66}N_6Zn_2BrCl_2^+$ 1223.2451, Found 1223.2467. Anal. Calcd for $C_{66}H_{66}N_6Zn_2Br_4$: C, 56.88; H, 4.77; N, 6.03. Found: C, 55.98; H, 5.06; N, 6.01.

(1)Co_2Br_4. A vial was charged with $CoBr_2$ (23.2 mg, 0.106 mmol, 2 equiv) and THF (5 mL). The suspension was stirred for ca. 5 min, resulting in a blue solution. **1** (50.0 mg, 0.053 mmol, 1 equiv) was added in one portion, resulting in a brown solution. The mixture was stirred for 16 h. Et_2O (10 mL) was added to the brown suspension and the mixture was stirred for ca. 5 min. The suspension was filtered through a sintered glass frit and the brown solid was washed with Et_2O (2 x 5 mL) and hexanes (5 mL), and dried under vacuum overnight to yield (**1**)Co_2Br_4 as a pale brown solid. Yield: 60.2 mg, 82.2 %. ^{1}H NMR (CD_2Cl_2, 500 MHz): δ 119.2 ($\upsilon_{1/2}$ = 1,000 Hz), 97.0 ($\upsilon_{1/2}$ = 1,000 Hz), 17.2 ($\upsilon_{1/2}$ = 2,000 Hz), 5.2 ($\upsilon_{1/2}$ = 80 Hz), 3.8 ($\upsilon_{1/2}$ = 30 Hz), 2.1 ($\upsilon_{1/2}$ = 30 Hz), 1.9 ($\upsilon_{1/2}$ = 20 Hz), 1.3 ($\upsilon_{1/2}$ = 30 Hz), 0.9 ($\upsilon_{1/2}$ = 30 Hz), 0.1 ($\upsilon_{1/2}$ = 200 Hz), -17.7 ($\upsilon_{1/2}$ = 1,000 Hz), -20.1 ($\upsilon_{1/2}$ = 1,000 Hz), -42.7 ($\upsilon_{1/2}$ = 1,000 Hz), -55.4 ($\upsilon_{1/2}$ = 1,000 Hz), -85.6 ($\upsilon_{1/2}$ = 1,000 Hz). MALDI-TOF-TOF (Dithranol) (m/z): [M-Br]$^+$ Calcd for $C_{66}H_{66}N_6Co_2Br_3^+$ 1301.15, Found 1301.15. ESI/APCI-TOF HRA-MS (m/z): [M-4Br+3Cl]$^+$ Calcd for $C_{66}H_{66}N_6Co_2Cl_3^+$ 1167.3064, Found 1167.3084; [M-3Br+2Cl]$^+$, Calcd for $C_{66}H_{66}N_6Co_2BrCl_2^+$ 1211.2556, Found 1211.2572; [M-2Br+Cl]$^+$ Calcd for $C_{66}H_{66}N_6Co_2Br_2Cl^+$ 1255.2050, Found 1255.2034. Anal. Calcd for $C_{66}H_{66}N_6Co_2Br_4$: C, 57.41; H, 4.82; N, 6.09. Found: C, 54.33; H, 5.33; N, 5.93. μ_{eff} (Evans method): 7.8(7) BM.

(1)Fe_2Br_4. A vial was charged with $FeBr_2$ (22.9 mg, 0.106 mmol, 2 equiv) and THF (10 mL). The suspension was stirred for 5 min, resulting in a yellow solution. **1** (50.0 mg, 0.053 mmol, 1 equiv) was added in one portion. The dark blue solution was stirred for 16 h. Et_2O (10 mL) was added and the mixture was stirred for ca. 5 min. The blue suspension was filtered through a sintered glass frit and the solid was washed with Et_2O (2 x 5 mL) and hexanes (5 mL) and dried under vacuum overnight to yield (**1**)Fe_2Br_4 as a dark blue solid. Yield: 54.1 mg, 74.2 %. ^{1}H NMR (CD_2Cl_2, 500 MHz): δ 11.3 ($\upsilon_{1/2}$ = 140 Hz), 6.0 ($\upsilon_{1/2}$ = 630 Hz), 3.7 ($\upsilon_{1/2}$ = 19.1), 2.8 ($\upsilon_{1/2}$ = 35 Hz), 2.2 ($\upsilon_{1/2}$ = 50 Hz), 1.2 ($\upsilon_{1/2}$ = 160 Hz), 0.8 ($\upsilon_{1/2}$ =), -15.1 ($\upsilon_{1/2}$ = 82 Hz), -21.7 ($\upsilon_{1/2}$ = 340 Hz). MALDI-TOF-TOF (Dithranol) (m/z): [M-Br]$^+$ Calcd for $C_{66}H_{66}N_6Fe_2Br_3^+$ 1295.16, Found 1295.16. ESI/APCI-TOF HRA-MS (m/z): [M-4Br+3Cl]$^+$ Calcd for $C_{66}H_{66}N_6Fe_2Cl_3^+$ 1161.3103; Found 1161.3108. Anal. Calcd for $C_{66}H_{66}N_6Fe_2Br_4$: C, 57.67; H, 4.84; N, 6.11. Found: C, 51.76; H, 5.06; N, 5.08. μ_{eff} (Evans method): 8.4(7) BM.

(2)Zn_2Br_4. A vial was charged with $ZnBr_2$ (67.6 mg, 0.300 mmol, 2 equiv) and THF (10 mL). The suspension was stirred for ca. 5 min, resulting in a pale-yellow solution. **2** (150.0 mg, 0.150 mmol, 1 equiv) was added in one portion. The yellow solution was stirred for 16 h. Et_2O (10 mL) was added and the mixture was stirred for ca. 5 min. The suspension was filtered through a sintered glass frit and the yellow solid was washed with Et_2O (3 x 10 mL) and hexanes (10 mL), and dried under vacuum for 2 d at 100 °C to yield (**2**)Zn_2Br_4 as a yellow solid. Yield: 181.6 mg, 83.0 %. The atom labelling scheme for (**2**)Zn_2Br_4 is shown in Figure 8. ^{1}H NMR (CD_2Cl_2, 500 MHz): δ 8.16 (s, 2H, H_f), 7.96 (s, 2H, H_f'), 7.36 (s, 2H, H_e'), 7.27 (m, 6 H, H_a, H_c', H_d'), 7.01 (s, 2H, H_e), 6.85 (d, $^3J_{HH}$ = 7.8 Hz, 2H, H_c), 6.50 (dd, $^3J_{HH}$ = 7.8 Hz, $^4J_{HH}$ = 1.2 Hz, 2H, H_d), 6.42 (s, 2H, H_a'), 2.36 (s, 6H, N=C-CH_3), 2.31 (s, 6H, terphenyl-Me'), 2.24 (s, 6H, terphenyl-Me), 2.19 (s, 6H, Me$_b$'), 2.04 (s, 6H, Me$_b$), 2.03 (s, 6H, N=C-CH_3'), 1.49 (s, 9H, ^{t}Bu), 1.44 (s, 9H, ^{t}Bu'). ^{13}C{^{1}H} NMR (CD_2Cl_2, 126 MHz): δ 164.2 (N=*C*'), 163.6 (N=*C*), 149.0, 148.1, 146.4, 145.6, 141.2, 138.5, 137.6, 137.4, 136.7, 136.0, 132.1 (*C*-H_e), 132.0 (*C*-H_e'), 130.4 (*C*-H_a or *C*-H_c' or *C*-H_d'), 129.6 (*C*- H_b), 127.6 (*C*-H_d), 126.6, 126.1 (*C*-H_a' overlapped with *C*-H_a or *C*-H_c' or *C*-H_d'), 125.2, 123.9 (*C*-H_a or *C*-H_c' or *C*-H_d'), 123.6 (*C*-H_f and *C*-H_f'), 36.5 (-*C*(CH$_3$)$_3$), 36.2 (-*C*(CH$_3$)$_3$'), 30.60 (-C(*C*H$_3$)$_3$), 30.58 (-C(*C*H$_3$)$_3$') 19.5 (terphenyl-*C*H$_3$'), 19.4 (terphenyl-*C*H$_3$), 18.4 (Me$_b$'), 17.9 (Me$_b$), 17.8 (N=C-*C*H$_3$'), 17.4 (N=C-*C*H$_3$). In total, 32 resonances are observed in ^{13}C{^{1}H} NMR and 36 are expected. Based on expected chemical shift, the 4 missing resonances correspond to the two sets of *o*-py and *p*-py quaternary carbons. This is due to low signal in ^{13}C{^{1}H} NMR due to the poor solubility of (**2**)Zn_2Br_4 in $C_2D_2Cl_4$. MALDI-TOF-TOF (Dithranol) (m/z): [M-Br]$^+$ Calcd for $C_{70}H_{74}N_6Zn_2Br_3^+$ 1369.21, Found 1369.20. ESI/APCI-TOF HRA-MS (m/z): [M-4Br+3Cl]$^+$ Calcd for $C_{70}H_{74}N_6Zn_2Cl_3^+$ 1235.3584, Found 1235.3634. Anal. Calcd for $C_{70}H_{74}N_6Zn_2Br_4$: C, 57.99; H, 5.15; N, 5.80. Found: C, 56.68; H, 5.06; N, 5.71.

(2)Co_2Br_4. This compound was synthesized by the procedure for (**1**)Co_2Br_4 using $CoBr_2$ (65.6 mg, 0.300 mmol, 2 equiv), **2** (150.0 mg, 0.150 mmol, 1 equiv), and THF (10 mL) The crude brown solid was washed with Et_2O (3 x 10 mL) and hexanes (10 mL), and dried under vacuum overnight to yield (**2**)Co_2Br_4 as a pale brown solid. Yield: 187.4 mg, 87.0 %. ^{1}H NMR (CD_2Cl_2, 500 MHz): δ 108.6 ($\upsilon_{1/2}$ = 200 Hz), 104.5 ($\upsilon_{1/2}$ = 130 Hz), 20.5 ($\upsilon_{1/2}$ = 71 Hz), 13.5 ($\upsilon_{1/2}$ = 61 Hz), 12.0 ($\upsilon_{1/2}$ = 100 Hz), 7.2 ($\upsilon_{1/2}$ = 71 Hz), 5.9 ($\upsilon_{1/2}$ = 130 Hz), -2.0 ($\upsilon_{1/2}$ = 56 Hz), -4.8 ($\upsilon_{1/2}$ = 71 Hz), -5.9 ($\upsilon_{1/2}$ = 59 Hz), -7.6 ($\upsilon_{1/2}$ = 110 Hz), -10.0 ($\upsilon_{1/2}$ = 59 Hz), -20.0 ($\upsilon_{1/2}$ = 210 Hz), -23.2 ($\upsilon_{1/2}$ = 93 Hz), -28.6 ($\upsilon_{1/2}$ = 190 Hz), -73.1 ($\upsilon_{1/2}$ = 300 Hz). MALDI-TOF-TOF (Dithranol) (m/z): [M-Br]$^+$ Calcd for $C_{70}H_{74}N_6Co_2Br_3^+$ 1357.22, Found 1357.21. ESI/APCI-TOF HRA-MS (m/z): [M-4Br+3Cl]$^+$ Calcd for $C_{70}H_{74}N_6Co_2Cl_3^+$ 1223.3692, Found 1223.3702; [M-3Br+2Cl]$^+$ Calcd for $C_{70}H_{74}N_6Co_2BrCl_2^+$ 1267.3184, Found 1267.3164. Anal. Calcd for $C_{70}H_{74}N_6Co_2Br_4$: C, 58.51; H, 5.21; N, 5.87. Found: C, 57.85; H, 5.12; N, 5.86.

(2)Fe_2Br_4. This compound was synthesized by the procedure for (**1**)Fe_2Br_4 using $FeBr_2$ (64.7 mg, 0.300 mmol, 2 equiv), **2** (150.0 mg, 0.150 mmol, 1 equiv), and THF (10 mL). The crude blue solid was washed with Et_2O (3 x 10 mL) and hexanes (10 mL), and dried under vacuum overnight to yield (**2**)Fe_2Br_4 as a dark blue solid. Yield: 154.3 mg, 72.0 %. ^{1}H NMR (CD_2Cl_2, 500 MHz): δ 79.0 ($\upsilon_{1/2}$ = 69 Hz), 75.0 ($\upsilon_{1/2}$ = 59 Hz), 12.5 ($\upsilon_{1/2}$ = 29 Hz), 11.6 ($\upsilon_{1/2}$ = 29 Hz), 9.8 ($\upsilon_{1/2}$ = 100 Hz), 8.3 ($\upsilon_{1/2}$ = 37 Hz), 8.0 ($\upsilon_{1/2}$ = 53 Hz), 7.8 ($\upsilon_{1/2}$ = 100 Hz), 5.0 ($\upsilon_{1/2}$ = 24 Hz), 4.0 ($\upsilon_{1/2}$ = 20 Hz), 0.6 ($\upsilon_{1/2}$ = 24 Hz), -1.43 ($\upsilon_{1/2}$ = 36 Hz), -8.3 ($\upsilon_{1/2}$ = 250 Hz), -12.3 ($\upsilon_{1/2}$ = 29 Hz), -17.6 ($\upsilon_{1/2}$ = 32 Hz), -23.2 ($\upsilon_{1/2}$ = 70 Hz), -25.8 ($\upsilon_{1/2}$ = 76 Hz). MALDI-TOF-TOF (Dithranol) (m/z): [M-Br]$^+$ Calcd for $C_{70}H_{74}N_6Fe_2Br_3^+$ 1351.22, Found 1351.19. ESI/APCI-TOF HRA-MS (m/z): [M-4Br+3Cl]$^+$ Calcd for $C_{70}H_{74}N_6Fe_2Cl_3^+$ 1217.3731; Found 1217.3750. Anal. Calcd for $C_{70}H_{74}N_6Fe_2Br_4$: C, 58.77; H, 5.21; N, 5.87. Found: C, 58.05; H, 5.31; N, 5.68.

(3)Zn_2Br_4. This compound was synthesized by the procedure for (**2**)Zn_2Br_4 using $ZnBr_2$ (60.8 mg, 0.270 mmol, 2 equiv), **3** (150.0 mg, 0.135 mmol, 1 equiv), and THF (10 mL). The crude solid was washed with Et_2O (3 x 10 mL) and hexanes (10 mL) and dried under vacuum for 2 d at 100 °C to yield (**3**)Zn_2Br_4 as a bright-yellow solid. Yield: 157.1 mg, 74.5 %. The atom labelling scheme for (**3**)Zn_2Br_4 is shown in Figure 8. ^{1}H NMR (CD_2Cl_2, 500 MHz): δ 8.23 (s, 2H), 8.01 (br s, 2H), 7.44 (br s, 4H), 7.35 (s, 3H), 7.06 (d, $^3J_{HH}$ = 7.9 Hz, 3H), 6.94 (br s, 2H), 6.71 (br s, 2H), 6.34 (br s, 2H), 2.89 (br s, 2H), 2.47 (s, 6H), 2.29 (s, 6H), 2.23 (s, 8H), 2.12 (br s, 4H), 1.52 (s, 9H), 1.43 (s, 9H), 1.18 (m, 24H). ^{1}H NMR ($C_2D_2Cl_4$, 500 MHz, 100 °C): δ 8.30 (s, 2H, H_f), 8.08 (s, 2H, H_f'), 7.57 (d, $^3J_{HH}$ = 8.0 Hz, 2H, H_c), 7.49 (d, $^3J_{HH}$ = 8.0 Hz, 2H, H_d), 7.39 (s, 2H, H_a), 7.34 (s, 2H, H_e), 7.11 (d, $^3J_{HH}$ = 7.5 Hz, 2H, H_c'), 6.99 (s, 2H, H_e'), 6.85 (d, $^3J_{HH}$ = 7.5 Hz, 2H, H_d'), 6.33 (s, 2H, H_a'), 2.75 (br s, 4H, -C*H*(CH$_3$)$_2$), 2.54 (s, 6H, N=C-CH_3), 2.36 (s, 6H, Me$_b$), 2.31 (s, 6H, Me$_b$'), 2.24 (s, 6H, N=C-CH_3'), 1.63 (s, 9H, ^{t}Bu), 1.52 (s, 9H, ^{t}Bu'), 1.27 (m, 24H, -CH(CH_3)$_2$). ^{13}C{^{1}H} NMR ($C_2D_2Cl_4$, 500 MHz, 100 °C): δ 164.4 (*C*-H_f), 148.6, 148.0, 144.3, 142.6, 140.8, 138.6, 137.0, 136.3, 136.2, 136.0, 135.7, 135.5, 132.4

(*C*-H$_e$'), 132.0 (*C*-H$_e$), 128.0 (*C*-H$_d$'), 127.4 (*C*-H$_d$), 126.9 (*C*-H$_c$), 124.9 (*C*-H$_c$'), 123.5 (*C*-H$_e$'), 123.2 (*C*-H$_e$), 36.3 (-*C*(CH$_3$)$_3$), 36.1 (-*C*(CH$_3$)$_3$'), 30.4 (-C(*C*H$_3$)$_3$), 30.2 (-C(*C*H$_3$)$_3$'), 27.6 (-*C*H(CH$_3$)$_2$), 27.4 (-*C*H(CH$_3$)$_2$), 24.9 (-CH(*C*H$_3$)$_2$), 24.4 (-CH(*C*H$_3$)$_2$'), 23.6 (-CH(*C*H$_3$)$_2$), 23.4 (-CH(*C*H$_3$)$_2$'), 18.83 (Me^1), 18.80 (Me$^{1'}$), 17.84 (Me$^{2'}$), 17.80 (Me^2). In total, 35 resonances are observed by $^{13}C\{^1H\}$ NMR and 38 resonances are expected. One N=*C* resonance is not observed. The other missing resonances correspond to the substituted aromatic carbons: *C*$_{terphenyl}$-C$_{aniline}$, C$_{terphenyl}$-*C*$_{aniline}$, and/or *o*-py and/or *p*-py. This is due to low signal in $^{13}C\{^1H\}$ NMR due to the poor solubility of (**3**)Zn$_2$Br$_4$ in C$_2$D$_2$Cl$_4$. MALDI-TOF-TOF (Dithranol) (m/z): $[M-Br]^+$ Calcd for $C_{78}H_{90}N_6Zn_2Br_3^+$ 1481.33, Found 1481.33. ESI/APCI-TOF HRA-MS (m/z): $[M-4Br+3Cl]^+$ Calcd for $C_{78}H_{90}N_6Zn_2Cl_3^+$ 1347.4839, Found 1347.4892; $[M-3Br+2Cl]^+$ Calcd for $C_{78}H_{90}N_6Zn_2BrCl_2^+$ 1393.4320, Found 1393.4376. Anal. Calcd for $C_{78}H_{90}N_6Zn_2Br_4$: C, 59.98; H, 5.81; N, 5.38. Found: C, 51.50; H, 5.46; N, 4.48.

(3)Co$_2$Br$_4$. This compound was synthesized by the procedure used for (**1**)Co$_2$Br$_4$ using CoBr$_2$ (59.1 mg, 0.270 mmol, 2 equiv), **3** (150.0 mg, 0.270 mmol, 1 equiv), and THF (10 mL). The crude solid was washed with Et$_2$O (3 x 10 mL) and hexanes (10 mL), and dried under vacuum overnight to yield (**3**)Co$_2$Br$_4$ as a pale brown solid. Yield: 170.1 mg, 81.3 %. ^{1}H NMR (CD$_2$Cl$_2$, 500 MHz): δ 119.0 ($\upsilon_{1/2}$ = 170 Hz), 108.7 ($\upsilon_{1/2}$ = 100 Hz), 18.2 ($\upsilon_{1/2}$ = 110 Hz), 16.4 ($\upsilon_{1/2}$ = 72 Hz), 14.8 ($\upsilon_{1/2}$ = 30 Hz), 14.4 ($\upsilon_{1/2}$ = 70 Hz), 6.6 ($\upsilon_{1/2}$ = 90 Hz), 4.0 ($\upsilon_{1/2}$ = 34 Hz), 0.93 ($\upsilon_{1/2}$ = 77 Hz), -5.0 ($\upsilon_{1/2}$ = 42 Hz), -5.1 ($\upsilon_{1/2}$ = 32 Hz), -5.5 ($\upsilon_{1/2}$ = 30 Hz), -14.0 ($\upsilon_{1/2}$ = 60 Hz), -14.1 ($\upsilon_{1/2}$ = 31 Hz), -19.8 ($\upsilon_{1/2}$ = 30 Hz), -23.0 ($\upsilon_{1/2}$ = 130 Hz), -28.1 ($\upsilon_{1/2}$ = 290 Hz), -30.2 ($\upsilon_{1/2}$ = 160 Hz), -49.7 ($\upsilon_{1/2}$ = 290 Hz), -63.1 ($\upsilon_{1/2}$ = 270 Hz), -87.9 ($\upsilon_{1/2}$ = 290 Hz). MALDI-TOF-TOF (Dithranol) (m/z): $[M-Br]^+$ Calcd for $C_{78}H_{90}N_6Co_2Br_3^+$ 1469.34, Found 1469.33. ESI/APCI-TOF HRA-MS (m/z): $[M-4Br+3Cl]^+$ Calcd for $C_{78}H_{90}N_6Co_2Cl_3^+$ 1335.4948, Found 1335.4988. Anal. Calcd for $C_{78}H_{90}N_6Co_2Br_4$: C, 60.48; H, 5.86; N, 5.43. Found: C, 66.47; H, 6.58; N, 5.90. μ_{eff} (Evans method): 7.9(8) BM.

(3)Fe$_2$Br$_4$. This compound was synthesized by the procedure for (**1**)Fe$_2$Br$_4$ using FeBr$_2$ (58.2 mg, 0.270 mmol, 2 equiv), **3** (150.0 mg, 0.135 mmol, 1 equiv), and THF (10 mL). The crude blue solid was washed with Et$_2$O (3 x 10 mL) and hexanes (10 mL), and dried under vacuum overnight to yield (**3**)Fe$_2$Br$_4$ as a dark blue solid. Yield: 153.8 mg, 73.8 %. ^{1}H NMR (CD$_2$Cl$_2$, 500 MHz): δ 76.8 ($\upsilon_{1/2}$ = 130 Hz), 74.7 ($\upsilon_{1/2}$ = 190 Hz), 13.8 ($\upsilon_{1/2}$ = 150 Hz), 12.2 ($\upsilon_{1/2}$ = 96 Hz), 7.0 ($\upsilon_{1/2}$ = 180 Hz), 5.3 ($\upsilon_{1/2}$ = 130 Hz), 4.3 ($\upsilon_{1/2}$ = 150 Hz), 2.7 ($\upsilon_{1/2}$ = 80 Hz), 1.6 ($\upsilon_{1/2}$ = 49 Hz), -0.2 ($\upsilon_{1/2}$ = 80 Hz), -2.9 ($\upsilon_{1/2}$ = 140 Hz), -5.2 ($\upsilon_{1/2}$ = 160 Hz), -10.1 ($\upsilon_{1/2}$ = 100 Hz), -16.4 ($\upsilon_{1/2}$ = 490 Hz), -17.2 ($\upsilon_{1/2}$ = 110 Hz), -17.3 ($\upsilon_{1/2}$ = 280 Hz), -18.7 ($\upsilon_{1/2}$ = 240 Hz), 18.9 ($\upsilon_{1/2}$ = 240 Hz), -24.4 ($\upsilon_{1/2}$ = 290 Hz), -28.7 ($\upsilon_{1/2}$ = 190 Hz). MALDI-TOF-TOF (Dithranol) (m/z): $[M-Br]^+$ Calcd for $C_{78}H_{90}N_6Fe_2Br_3^+$ 1463.35, Found 1463.34. ESI/APCI-TOF HRA-MS (m/z): $[M-4Br+3Cl]^+$ Calcd for $C_{78}H_{90}N_6Fe_2Cl_3^+$ 1329.4987, Found 1329.5024. Anal. Calcd for $C_{78}H_{90}N_6Fe_2Br_4$: C, 60.72; H, 5.88; N, 5.45. Found: C, 58.63; H, 5.69; N, 5.50. μ_{eff} (Evans method): 8.9(5) BM.

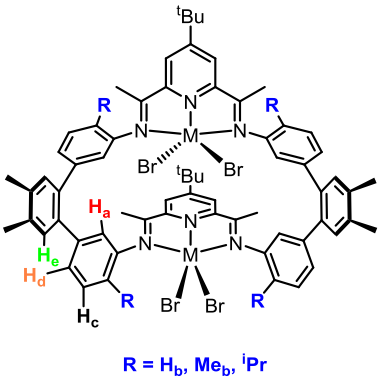

Figure 7. Atom labelling scheme for (**1-3**)M$_2$Br$_4$ under conditions of fast PDI exchange.

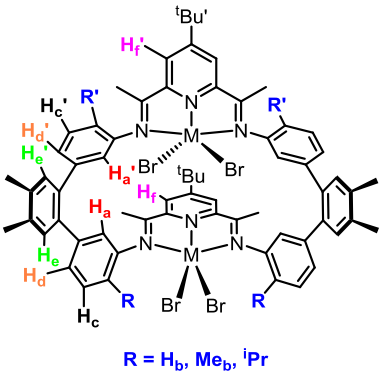

Figure 8. Atom labelling scheme for (**1-3**)M$_2$Br$_4$ under conditions of slow PDI exchange.

Low pressure ethylene oligomerization. Ethylene oligomerization/polymerization reactions at 2 bar were performed in a 200 mL Fischer-Porter bottle equipped with a 2-inch long Teflon-coated magnetic stir bar and a stainless-steel pressure head fitted with inlet and outlet needle valves, a septum-capped ball valve for injections, a safety check valve, and a pressure gauge. In a N$_2$-filled glovebox, the Fischer-Porter bottle was charged with PhMe (46.5 mL) and a catalyst stock suspension in PhMe (1.0 mL). The apparatus was removed from the glovebox, connected to a stainless-steel double manifold vacuum/ethylene line, placed in a room temperature water bath and stirred at 370 rpm. The N$_2$ atmosphere was replaced with ethylene by three evacuation-refill cycles. The solution was equilibrated at 2 bar of ethylene pressure for 15 min. A stock solution of the appropriate Al activator in PhMe (2.5 mL) was added via gas-tight syringe. The ethylene pressure was kept constant by feeding ethylene on demand. Ethylene consumption was measured using a Brooks Instruments 5860i Mass Flow Sensor. The total ethylene consumption was determined by numerical integration of the mass flow curve using the LabView software package. After 30 min, the ethylene line was closed, the Fischer-Porter bottle was vented and MeOH (50 mL) was added to quench the reaction. *o*-Xylene (100 μL) was added as an internal standard, and the solution was analyzed by GC-MS using an Aglient 6890/5973N GC-MS instrument. The masses of the oligomers were determined by GC-MS using predetermined response factors.

High pressure ethylene polymerization reactions. Ethylene polymerizations at 20 bar were performed using a stainless-steel Parr 300 mL autoclave, which was equipped with a magnetically driven 1.5-inch diameter four-blade propeller stirrer, thermocouple, water cooling loop, and a Parr 4842 controller. In a N$_2$ glovebox, a 200 mL glass autoclave liner was charged with PhMe (39.0 mL) and a stock suspension of the catalyst in PhMe (1.0 mL) and placed in the autoclave. The autoclave was sealed, removed from the glovebox, and attached to the ethylene line. A stock solution of the appropriate Al activator in PhMe (2.5 mL) was transferred to a 10 mL stainless-steel

injection port and diluted with PhMe (7.5 mL) The mixture was stirred (400 rpm), pressurized to 15 bar of ethylene, and stirred at the desired reaction temperature for 15 min. The injection line was attached, and the activator solution injected at 20 bar. The ethylene pressure was kept constant by feeding ethylene on demand. After 30 min the ethylene line was closed, and the autoclave was vented. Methanol (50 mL) was added to precipitate the polymer, which was characterized as described below.

Polymer Analysis. DSC measurements were performed on a TA Instruments 2920 differential scanning calorimeter. Samples (5 mg) were annealed by heating to 250 ºC at 15 C/min, cooled to 0 ºC at 10 °C/min, and analyzed by heating to 250 °C at 15 °C/min. ^{1}H and ^{13}C{^{1}H} NMR spectra of PE samples were obtained at 100 ºC in dry degassed $CDCl_2CDCl_2$ solvent using a Bruker Advance 500 NMR instrument. ^{13}C{^{1}H} NMR spectra of PE samples were internally referenced to the main-chain CH_2 resonance at δ 30.0. Gel permeation chromatography (GPC) was performed on a Polymer Laboratories PL−GPC 200 instrument at 150 °C with 1,2,4-trichlorobenzene (stabilized with 125 ppm BHT) as the mobile phase. Three PLgel 10 μm Mixed-B LS columns were used. The molecular weights were calibrated using narrow polystyrene standards with a 10-point calibration of M_n from 570 Da to 5670 kDa, and are corrected for linear polyethylene by universal calibration by using the following Mark−Houwink parameters: polystyrene, $K = 1.75 \times 10{-}2$ cm^3 g^{-1} , $\alpha = 0.67$; polyethylene, $K = 5.90 \times 10^{-2}$ cm^3 g^{-1} , $\alpha = 0.69$.[72]

ASSOCIATED CONTENT

Supporting Information

The Supporting Information is available free of charge on the ACS Publications website.

NMR and mass spectra for compounds, GPC and and NMR of polymers, X-ray crystallography details (PDF)

Accession Codes. CCDC 1991375-1991379 contain the supplementary crystallographic data for this paper. These data can be obtained free of charge via www.ccdc.cam.ac.uk/data_request/cif, or by emailing data_request@ccdc.cam.ac.uk, or by contacting The Cambridge Crystallographic Data Centre, 12, Union Road, Cambridge CB2 1EZ, UK; fax: +44 1223 336033

AUTHOR INFORMATION

Corresponding Author

*rfjordan@uchicago.edu.

ORCID

Erik D. Reinhart: **0000-0003-2878-9376**
Richard F. Jordan: **0000-0002-3158-4745**

Funding Sources

This work was supported by the National Science Foundation (NSF) under grant number CHE-1709159.

Notes

The authors declare no competing financial interest

ACKNOWLEDGMENT

We thank Dr. Antoni Jurkiewicz and Dr. Josh Kurutz for assistance with NMR, Dr. Alexander Filatov and Andrew McNeece for assistance with X-ray crystallography, and Dr. Chang Qin for assistance with mass spectrometry.

REFERENCES

(1) Small, B. L.; Brookhart, M.; Bennett, A. M. A. Highly Active Iron and Cobalt Catalysts for the Polymerization of Ethylene. *J. Am. Chem. Soc.* **1998**, *120* (16), 4049–4050. https://doi.org/10.1021/ja9802100.

(2) Britovsek, G. J. P.; Bruce, M.; Gibson, V. C.; Kimberley, B. S.; Maddox, P. J.; Mastroianni, S.; McTavish, S. J.; Redshaw, C.; Solan, G. A.; Strömberg, S.; White, A. J. P.; Williams, D. J. Iron and Cobalt Ethylene Polymerization Catalysts Bearing 2,6-Bis(Imino)Pyridyl Ligands: Synthesis, Structures, and Polymerization Studies. *J. Am. Chem. Soc.* **1999**, *121* (38), 8728–8740. https://doi.org/10.1021/ja990449w.

(3) Gibson, V. C.; Redshaw, C.; Solan, G. A. Bis(Imino)Pyridines: Surprisingly Reactive Ligands and a Gateway to New Families of Catalysts. *Chem. Rev.* **2007**, *107* (5), 1745–1776. https://doi.org/10.1021/cr068437y.

(4) Small, B. L. Discovery and Development of Pyridine-Bis(Imine) and Related Catalysts for Olefin Polymerization and Oligomerization. *Acc. Chem. Res.* **2015**, *48* (9), 2599–2611. https://doi.org/10.1021/acs.accounts.5b00252.

(5) Flisak, Z.; Sun, W.-H. Progression of Diiminopyridines: From Single Application to Catalytic Versatility. *ACS Catal.* **2015**, *5* (8), 4713–4724. https://doi.org/10.1021/acscatal.5b00820.

(6) Wang, Z.; Solan, G. A.; Zhang, W.; Sun, W.-H. Carbocyclic-Fused N,N,N-Pincer Ligands as Ring-Strain Adjustable Supports for Iron and Cobalt Catalysts in Ethylene Oligo-/Polymerization. *Coord. Chem. Rev.* **2018**, *363*, 92–108. https://doi.org/10.1016/j.ccr.2018.02.016.

(7) Mukhopadhyay, T. K.; Rock, C. L.; Hong, M.; Ashley, D. C.; Groy, T. L.; Baik, M.-H.; Trovitch, R. J. Mechanistic Investigation of Bis(Imino)Pyridine Manganese Catalyzed Carbonyl and Carboxylate Hydrosilylation. *J. Am. Chem. Soc.* **2017**, *139* (13), 4901–4915. https://doi.org/10.1021/jacs.7b00879.

(8) Schuster, C. H.; Diao, T.; Pappas, I.; Chirik, P. J. Bench-Stable, Substrate-Activated Cobalt Carboxylate Pre-Catalysts for Alkene Hydrosilylation with Tertiary Silanes. *ACS Catal.* **2016**, *6* (4), 2632–2636. https://doi.org/10.1021/acscatal.6b00304.

(9) Hojilla Atienza, C. C.; Tondreau, A. M.; Weller, K. J.; Lewis, K. M.; Cruse, R. W.; Nye, S. A.; Boyer, J. L.; Delis, J. G. P.; Chirik, P. J. High-Selectivity Bis(Imino)Pyridine Iron Catalysts for the Hydrosilylation of 1,2,4-Trivinylcyclohexane. *ACS Catal.* **2012**, *2* (10), 2169–2172. https://doi.org/10.1021/cs300584b.

(10) Tondreau, A. M.; Atienza, C. C. H.; Weller, K. J.; Nye, S. A.; Lewis, K. M.; Delis, J. G. P.; Chirik, P. J. Iron Catalysts for Selective Anti-Markovnikov Alkene Hydrosilylation Using Tertiary Silanes. *Science* **2012**, *335* (6068), 567–570. https://doi.org/10.1126/science.1214451.

(11) Obligacion, J. V.; Chirik, P. J. Highly Selective Bis(Imino)Pyridine Iron-Catalyzed Alkene Hydroboration. *Org. Lett.* **2013**, *15* (11), 2680–2683. https://doi.org/10.1021/ol400990u.

(12) Obligacion, J. V.; Chirik, P. J. Bis(Imino)Pyridine Cobalt-Catalyzed Alkene Isomerization–Hydroboration: A Strategy for Remote Hydrofunctionalization with Terminal Selectivity. *J. Am. Chem. Soc.* **2013**, *135* (51), 19107–19110. https://doi.org/10.1021/ja4108148.

(13) Obligacion, J. V.; Neely, J. M.; Yazdani, A. N.; Pappas, I.; Chirik, P. J. Cobalt Catalyzed Z-Selective Hydroboration of Terminal Alkynes and Elucidation of the Origin of Selectivity. *J. Am. Chem. Soc.* **2015**, *137* (18), 5855–5858. https://doi.org/10.1021/jacs.5b00936.

(14) Obligacion, J. V.; Chirik, P. J. Earth-Abundant Transition Metal Catalysts for Alkene Hydrosilylation and Hydroboration. *Nat. Chem. Rev.* **2018**, *2* (5), 15–34. https://doi.org/10.1038/s41570-018-0001-2.

(15) Bouwkamp, M. W.; Bowman, A. C.; Lobkovsky, E.; Chirik, P. J. Iron-Catalyzed [2π + 2π] Cycloaddition of α,ω-Dienes: The Importance of Redox-Active Supporting Ligands. *J. Am. Chem. Soc.* **2006**, *128* (41), 13340–13341. https://doi.org/10.1021/ja064711u.

(16) Hoyt, J. M.; Schmidt, V. A.; Tondreau, A. M.; Chirik, P. J. Iron-Catalyzed Intermolecular [2+2] Cycloadditions of Unactivated Alkenes. *Science* **2015**, *349* (6251), 960–963. https://doi.org/10.1126/science.aac7440.

(17) Hoyt, J. M.; Sylvester, K. T.; Semproni, S. P.; Chirik, P. J. Synthesis and Electronic Structure of Bis(Imino)Pyridine Iron Metal-

lacyclic Intermediates in Iron-Catalyzed Cyclization Reactions. *J. Am. Chem. Soc.* **2013**, *135* (12), 4862–4877. https://doi.org/10.1021/ja400895j.

(18) Schmidt, V. A.; Hoyt, J. M.; Margulieux, G. W.; Chirik, P. J. Cobalt-Catalyzed [2π + 2π] Cycloadditions of Alkenes: Scope, Mechanism, and Elucidation of Electronic Structure of Catalytic Intermediates. *J. Am. Chem. Soc.* **2015**, *137* (24), 7903–7914. https://doi.org/10.1021/jacs.5b04034.

(19) Rummelt, S. M.; Zhong, H.; Korobkov, I.; Chirik, P. J. Iron-Mediated Coupling of Carbon Dioxide and Ethylene: Macrocyclic Metallalactones Enable Access to Various Carboxylates. *J. Am. Chem. Soc.* **2018**, *140* (37), 11589–11593. https://doi.org/10.1021/jacs.8b07558.

(20) Biernesser, A. B.; Li, B.; Byers, J. A. Redox-Controlled Polymerization of Lactide Catalyzed by Bis(Imino)Pyridine Iron Bis(Alkoxide) Complexes. *J. Am. Chem. Soc.* **2013**, *135* (44), 16553–16560. https://doi.org/10.1021/ja407920d.

(21) Manna, C. M.; Kaur, A.; Yablon, L. M.; Haeffner, F.; Li, B.; Byers, J. A. Stereoselective Catalysis Achieved through in Situ Desymmetrization of an Achiral Iron Catalyst Precursor. *J. Am. Chem. Soc.* **2015**, *137* (45), 14232–14235. https://doi.org/10.1021/jacs.5b09966.

(22) Biernesser, A. B.; Delle Chiaie, K. R.; Curley, J. B.; Byers, J. A. Block Copolymerization of Lactide and an Epoxide Facilitated by a Redox Switchable Iron-Based Catalyst. *Angew. Chem. Int. Ed.* **2016**, *55* (17), 5251–5254. https://doi.org/10.1002/anie.201511793.

(23) Chiaie, K. R. D.; Yablon, L. M.; Biernesser, A. B.; Michalowski, G. R.; Sudyn, A. W.; Byers, J. A. Redox-Triggered Crosslinking of a Degradable Polymer. *Polym. Chem.* **2016**, *7* (28), 4675–4681. https://doi.org/10.1039/C6PY00975A.

(24) Chiaie, K. R. D.; Biernesser, A. B.; Ortuño, M. A.; Dereli, B.; Iovan, D. A.; Wilding, M. J. T.; Li, B.; Cramer, C. J.; Byers, J. A. The Role of Ligand Redox Non-Innocence in Ring-Opening Polymerization Reactions Catalysed by Bis(Imino)Pyridine Iron Alkoxide Complexes. *Dalton Trans.* **2017**, *46* (38), 12971–12980. https://doi.org/10.1039/C7DT03067C.

(25) Ortuño, M. A.; Dereli, B.; Chiaie, K. R. D.; Biernesser, A. B.; Qi, M.; Byers, J. A.; Cramer, C. J. The Role of Alkoxide Initiator, Spin State, and Oxidation State in Ring-Opening Polymerization of ε-Caprolactone Catalyzed by Iron Bis(Imino)Pyridine Complexes. *Inorg. Chem.* **2018**, *57* (4), 2064–2071. https://doi.org/10.1021/acs.inorgchem.7b02964.

(26) Qi, M.; Dong, Q.; Wang, D.; Byers, J. A. Electrochemically Switchable Ring-Opening Polymerization of Lactide and Cyclohexene Oxide. *J. Am. Chem. Soc.* **2018**, *140* (17), 5686–5690. https://doi.org/10.1021/jacs.8b02171.

(27) Takeuchi, D.; Takano, S.; Takeuchi, Y.; Osakada, K. Ethylene Polymerization at High Temperatures Catalyzed by Double-Decker-Type Dinuclear Iron and Cobalt Complexes: Dimer Effect on Stability of the Catalyst and Polydispersity of the Product. *Organometallics* **2014**, *33* (19), 5316–5323. https://doi.org/10.1021/om500629a.

(28) Takano, S.; Takeuchi, Y.; Takeuchi, D.; Osakada, K. Selective Formation of Ethyl- and/or Propyl-Branched Oligoethylene Using Double-Decker-Type Dinuclear Fe Complexes as the Catalyst. *Chem. Lett.* **2013**, *43* (4), 465–467. https://doi.org/10.1246/cl.131065.

(29) Wang, L.; Sun, J. Methylene Bridged Binuclear Bis(Imino)Pyridyl Iron(II) Complexes and Their Use as Catalysts Together with Al(i-Bu)3 for Ethylene Polymerization. *Inorganica Chimica Acta* **2008**, *361* (7), 1843–1849. https://doi.org/10.1016/j.ica.2007.09.039.

(30) Suo, H.; Solan, G. A.; Ma, Y.; Sun, W.-H. Developments in Compartmentalized Bimetallic Transition Metal Ethylene Polymerization Catalysts. *Coord. Chem. Rev.* **2018**, *372*, 101–116. https://doi.org/10.1016/j.ccr.2018.06.006.

(31) Chen, Q.; Zhang, W.; Solan, G. A.; Zhang, R.; Guo, L.; Hao, X.; Sun, W.-H. CH(Phenol)-Bridged Bis(Imino)Pyridines as Compartmental Supports for Diiron Precatalysts for Ethylene Polymerization: Exploring Cooperative Effects on Performance. *Organometallics* **2018**, *37* (21), 4002–4014. https://doi.org/10.1021/acs.organomet.8b00602.

(32) Xing, Q.; Zhao, T.; Du, S.; Yang, W.; Liang, T.; Redshaw, C.; Sun, W.-H. Biphenyl-Bridged 6-(1-Aryliminoethyl)-2-Iminopyridylcobalt Complexes: Synthesis, Characterization, and Ethylene Polymerization Behavior. *Organometallics* **2014**, *33* (6), 1382–1388. https://doi.org/10.1021/om4010884.

(33) Xing, Q.; Zhao, T.; Qiao, Y.; Wang, L.; Redshaw, C.; Sun, W.-H. Synthesis, Characterization and Ethylene Polymerization Behavior of Binuclear Iron Complexes Bearing N,N′-Bis(1-(6-(1-(Arylimino)Ethyl) Pyridin-2-Yl)Ethylidene)Benzidines. *RSC Adv.* **2013**, *3* (48), 26184–26193. https://doi.org/10.1039/C3RA42631A.

(34) Liu, J.; Li, Y.; Liu, J.; Li, Z. Ethylene Polymerization with a Highly Active and Long-Lifetime Macrocycle Trinuclear 2,6-Bis(Imino)Pyridyliron. *Macromolecules* **2005**, *38* (7), 2559–2563. https://doi.org/10.1021/ma047685y.

(35) Salata, C. A.; Youinou, M. T.; Burrows, C. J. (Template)2 Synthesis of a Dinucleating Macrocyclic Ligand and Crystal Structure of Its Dicopper(II) Imidazolate Complex. *J. Am. Chem. Soc.* **1989**, *111* (26), 9278–9279. https://doi.org/10.1021/ja00208a048.

(36) Salata, C. A.; Youinou, M. Therese.; Burrows, C. J. Preparation and Structural Characterization of Dicopper(II) and Dinickel(II) Imidazolate-Bridged Macrocyclic Schiff Base Complexes. *Inorg. Chem.* **1991**, *30* (18), 3454–3461. https://doi.org/10.1021/ic00018a015.

(37) Beattie, J. W.; SantaLucia, D. J.; White, D. S.; Groysman, S. Oxalate-Templated Synthesis of Di-Zinc Macrocycles. *Inorg. Chim. Acta* **2017**, *460*, 8–16. https://doi.org/10.1016/j.ica.2016.02.063.

(38) Reinhart, E. D.; Jordan, R. F. Template-Free Synthesis of a Macrocyclic Bis(Pyridine-Dienamine) Proligand and Metal Complexes of Its Bis(Pyridine-Diimine) and Bis(Pyridine-Dienamido) Forms. *Inorg. Chem.* **2019**, *58* (22), 15466–15478. https://doi.org/10.1021/acs.inorgchem.9b02539.

(39) Burger has reported a dinuclear (bis-PDI)Zn_2Cl_4 complex linked by a 1,8-napthalene bridge between the *para* positions of the pyridine rings. They report a Zn-Zn distance of 5.9168(9) Å. (a) Dammann, W.; Buban, T.; Schiller, C.; Burger, P. Dinuclear Tethered Pyridine, Diimine Complexes. *Dalton Trans.* **2018**, *47* (35), 12105–12117. https://doi.org/10.1039/C8DT02347F. For complexes of macrocyclic bis-PDI ligands tethered by short alkyl linkers see: (b) Cui, P.; Wang, Q.; McCollom, S. P.; Manor, B. C.; Carroll, P. J.; Tomson, N. C. Ring-Size-Modulated Reactivity of Putative Dicobalt-Bridging Nitrides: C−H Activation versus Phosphinimide Formation. *Angew. Chem. Int. Ed.* **2017**, *56* (50), 15979–15983. https://doi.org/10.1002/anie.201708966. (c) Zhang, S.; Wang, Q.; Thierer, L. M.; Weberg, A. B.; Gau, M. R.; Carroll, P. J.; Tomson, N. C. Tuning Metal–Metal Interactions through Reversible Ligand Folding in a Series of Dinuclear Iron Complexes. *Inorg. Chem.* **2019**, *58* (18), 12234–12244. https://doi.org/10.1021/acs.inorgchem.9b01673. (d) Wang, Q.; Zhang, S.; Cui, P.; Weberg, A. B.; Thierer, L. M.; Manor, B. C.; Gau, M. R.; Carroll, P. J.; Tomson, N. C. Interdependent Metal–Metal Bonding and Ligand Redox-Activity in a Series of Dinuclear Macrocyclic Complexes of Iron, Cobalt, and Nickel. *Inorg. Chem.* **2019**. https://doi.org/10.1021/acs.inorgchem.9b02339.

(40) Hollingsworth, R. L.; Beattie, J. W.; Grass, A.; Martin, P. D.; Groysman, S.; Lord, R. L. Reactions of Dicobalt Octacarbonyl with Dinucleating and Mononucleating Bis(Imino)Pyridine Ligands. *Dalton Trans.* **2018**, *47* (43), 15353–15363. https://doi.org/10.1039/C8DT03405B.

(41) Fan, R.; Zhu, D.; Ding, H.; Mu, Y.; Su, Q.; Xia, H. Blue Luminescent Zinc(II) Complexes of 2,6-Bis[1-(2,6-Diisopropylphenylimino)Ethyl]Pyridine and 2,6-Bis[1-(2,6-Dimethylphenylimino)Ethyl]Pyridine. *Synth. Met.* **2005**, *149* (2), 135–141. https://doi.org/10.1016/j.synthmet.2004.12.016.

(42) The ^{1}H NMR spectrum of (**3**)Zn_2Br_4 is broad at room temperature due to hindered Ar-^{i}Pr bond rotation. At 100 °C, the ^{1}H NMR spectrum is sharper and contains one broad methine resonance for the ^{i}Pr units (two septets are expected for C_s-symmetric structures with fast Ar-^{i}Pr bond rotation).

(43) A total of 18 and 22 resonances respectively are expected in the ^{1}H NMR spectra of (**2**)M_2Br_4 and (**3**)M_2Br_4 for C_s-symmetric structures under conditions of slow exchange of the (PDI)M units. 16 and 17 ^{1}H resonances are observed for (**2**)Co_2Br_4 and (**2**)Fe_2Br_4 re-

spectively. The unobserved resonances are most likely broadened into the baseline. The ^{1}H NMR spectrum of (**3**)Co_2Br_4 contains the expected 22 resonances. The ^{1}H NMR spectrum of (**3**)Fe_2Br_4 contains 20 resonances due to overlapping of several resonances at δ -17.2 and 18.7.

(44) Britovsek, G. J. P.; Mastroianni, S.; Solan, G. A.; Baugh, S. P. D.; Redshaw, C.; Gibson, V. C.; White, A. J. P.; Williams, D. J.; Elsegood, M. R. J. Oligomerisation of Ethylene by Bis(Imino)Pyridyliron and -Cobalt Complexes. *Chem. Eur. J.* **2000**, *6* (12), 2221–2231. https://doi.org/10.1002/1521-3765(20000616)6:12<2221::AID-CHEM2221>3.0.CO;2-U.

(45) Hossain, Md. J.; Yamasaki, M.; Mikuriya, M.; Kuribayashi, A.; Sakiyama, H. Synthesis, Structure, and Magnetic Properties of Dinuclear Cobalt(II) Complexes with a New Phenol-Based Dinucleating Ligand with Four Hydroxyethyl Chelating Arms. *Inorg. Chem.* **2002**, *41* (15), 4058–4062. https://doi.org/10.1021/ic0255297.

(46) Weber, B.; Kaps, E. Synthesis and Magnetic Properties of New Dinuclear Iron(II) Complexes of a Phenylene-Bridge Shiff Base Analogue Dinucleating Ligand. *Heteroat. Chem.* **2005**, *16* (5), 391–397. https://doi.org/10.1002/hc.20108.

(47) Bryliakov, K. P.; Semikolenova, N. V.; Zakharov, V. A.; Talsi, E. P. Active Intermediates of Ethylene Polymerization over 2,6-Bis(Imino)Pyridyl Iron Complex Activated with Aluminum Trialkyls and Methylaluminoxane. *Organometallics* **2004**, *23* (22), 5375–5378. https://doi.org/10.1021/om0497184.

(48) Scott, J.; Gambarotta, S.; Korobkov, I.; Knijnenburg, Q.; de Bruin, B.; Budzelaar, P. H. M. Formation of a Paramagnetic Al Complex and Extrusion of Fe during the Reaction of (Diiminepyridine)Fe with AlR_3 (R = Me, Et). *J. Am. Chem. Soc.* **2005**, *127* (49), 17204–17206. https://doi.org/10.1021/ja056135s.

(49) Cartes, M. Á.; Rodríguez-Delgado, A.; Palma, P.; Álvarez, E.; Cámpora, J. Sequential Reduction and Alkyl Exchange Reactions of Bis(Imino)Pyridine Dialkyliron(II) with Trimethylaluminum. *Organometallics* **2014**, *33* (7), 1834–1839. https://doi.org/10.1021/om500167r.

(50) Velthoen, M. E. Z.; Muñoz-Murillo, A.; Bouhmadi, A.; Cecius, M.; Diefenbach, S.; Weckhuysen, B. M. The Multifaceted Role of Methylaluminoxane in Metallocene-Based Olefin Polymerization Catalysis. *Macromolecules* **2018**, *51* (2), 343–355. https://doi.org/10.1021/acs.macromol.7b02169.

(51) Endres, E.; Zijlstra, H. S.; Collins, S.; McIndoe, J. S.; Linnolahti, M. Oxidation of Methylalumoxane Oligomers: A Theoretical Study Guided by Mass Spectrometry. *Organometallics* **2018**, *37* (21), 3936–3942. https://doi.org/10.1021/acs.organomet.8b00587.

(52) Zijlstra, H. S.; Linnolahti, M.; Collins, S.; McIndoe, J. S. Additive and Aging Effects on Methylalumoxane Oligomers. *Organometallics* **2017**, *36* (9), 1803–1809. https://doi.org/10.1021/acs.organomet.7b00153.

(53) Imhoff, D. W.; Simeral, L. S.; Sangokoya, S. A.; Peel, J. H. Characterization of Methylaluminoxanes and Determination of Trimethylaluminum Using Proton NMR. *Organometallics* **1998**, *17* (10), 1941–1945. https://doi.org/10.1021/om980046p.

(54) Small, B. L.; Brookhart, M. Polymerization of Propylene by a New Generation of Iron Catalysts: Mechanisms of Chain Initiation, Propagation, and Termination. *Macromolecules* **1999**, *32* (7), 2120–2130. https://doi.org/10.1021/ma981698s.

(55) Bryliakov, K. P.; Semikolenova, N. V.; Zudin, V. N.; Zakharov, V. A.; Talsi, E. P. Ferrous Rather than Ferric Species Are the Active Sites in Bis(Imino)Pyridine Iron Ethylene Polymerization Catalysts. *Catal. Commun.* **2004**, *5* (1), 45–48. https://doi.org/10.1016/j.catcom.2003.11.010.

(56) Bryliakov, K. P.; Talsi, E. P.; Semikolenova, N. V.; Zakharov, V. A. Formation and Nature of the Active Sites in Bis(Imino)Pyridine Iron-Based Polymerization Catalysts. *Organometallics* **2009**, *28* (11), 3225–3232. https://doi.org/10.1021/om8010905.

(57) Semikolenova, N. V.; Zakharov, V. A.; Echevskaja, L. G.; Matsko, M. A.; Bryliakov, K. P.; Talsi, E. P. Homogeneous Catalysts for Ethylene Polymerization Based on Bis(Imino)Pyridine Complexes of Iron, Cobalt, Vanadium and Chromium. *Catalysis Today* **2009**, *144* (3), 334–340. https://doi.org/10.1016/j.cattod.2009.01.022.

(58) Semikolenova, N. V.; Sun, W.-H.; Soshnikov, I. E.; Matsko, M. A.; Kolesova, O. V.; Zakharov, V. A.; Bryliakov, K. P. Origin of "Multisite-like" Ethylene Polymerization Behavior of the Single-Site Nonsymmetrical Bis(Imino)Pyridine Iron(II) Complex in the Presence of Modified Methylaluminoxane. *ACS Catal.* **2017**, *7* (4), 2868–2877. https://doi.org/10.1021/acscatal.7b00486.

(59) Radhakrishnan, K.; Cramail, H.; Deffieux, A.; François, P.; Momtaz, A. Influence of Alkylaluminium Activators and Mixtures Thereof on Ethylene Polymerization with a Tridentate Bis(Imino)Pyridinyliron Complex. *Macromol. Rapid Commun.* **2003**, *24* (3), 251–254. https://doi.org/10.1002/marc.200390036.

(60) Wang, Q.; Yang, H.; Fan, Z. Efficient Activators for an Iron Catalyst in the Polymerization of Ethylene. *Macromol. Rapid Commun.* **2002**, *23* (10–11), 639–642. https://doi.org/10.1002/1521-3927(20020701)23:10/11<639::AID-MARC639>3.0.CO;2-A.

(61) Bent, B. E.; Nuzzo, R. G.; Dubois, L. H. Surface Organometallic Chemistry in the Chemical Vapor Deposition of Aluminum Films Using Triisobutylaluminum: .Beta.-Hydride and .Beta.-Alkyl Elimination Reactions of Surface Alkyl Intermediates. *J. Am. Chem. Soc.* **1989**, *111* (5), 1634–1644. https://doi.org/10.1021/ja00187a016.

(62) Pierson, H. O. Aluminum Coatings by the Decomposition of Alkyls. *Thin Solid Films* **1977**, *45* (2), 257–263. https://doi.org/10.1016/0040-6090(77)90258-9.

(63) Ziegler, K.; Kroll, W.-R.; Larbig, W.; Steudel, O.-W. Metallorganische Verbindungen, XXXII Zerfalls- Und Austauschreaktionen Der Aluminiumtrialkyle. *Justus Liebigs Annalen der Chemie* **1960**, *629* (1), 53–89. https://doi.org/10.1002/jlac.19606290108.

(64) Weliange, N. M.; McGuinness, D. S.; Gardiner, M. G.; Patel, J. Insertion, Elimination and Isomerisation of Olefins at Alkylaluminium Hydride: An Experimental and Theoretical Study. *Dalton Trans.* **2015**, *44* (34), 15286–15296. https://doi.org/10.1039/C5DT00955C.

(65) Egger, K. W. Kinetics of the Intramolecular Four-Center Elimination of Isobutylene from Triisobutylaluminum in the Gas Phase. *J. Am. Chem. Soc.* **1969**, *91* (11), 2867–2871. https://doi.org/10.1021/ja01039a007.

(66) Attempts to prepare (**1**-**3**)M_2Cl_4 complexes were unsuccessful.

(67) Hanton, M. J.; Tenza, K. Bis(Imino)Pyridine Complexes of the First-Row Transition Metals: Alternative Methods of Activation. *Organometallics* **2008**, *27* (21), 5712–5716. https://doi.org/10.1021/om800744j.

(68) Small, B. L.; Brookhart, M. Iron-Based Catalysts with Exceptionally High Activities and Selectivities for Oligomerization of Ethylene to Linear α-Olefins. *J. Am. Chem. Soc.* **1998**, *120* (28), 7143–7144. https://doi.org/10.1021/ja981317q.

(69) Nückel, S.; Burger, P. Transition Metal Complexes with Sterically Demanding Ligands, 3.1 Synthetic Access to Square-Planar Terdentate Pyridine−Diimine Rhodium(I) and Iridium(I) Methyl Complexes: Successful Detour via Reactive Triflate and Methoxide Complexes. *Organometallics* **2001**, *20* (21), 4345–4359. https://doi.org/10.1021/om010185y.

(70) Dilly, S.; Fotso Fotso, A.; Lejal, N.; Zedda, G.; Chebbo, M.; Rahman, F.; Companys, S.; Bertrand, H. C.; Vidic, J.; Noiray, M.; Alessi, M.-C.; Tarus, B.; Quideau, S.; Riteau, B.; Slama-Schwok, A. From Naproxen Repurposing to Naproxen Analogues and Their Antiviral Activity against Influenza A Virus. *J. Med. Chem.* **2018**, *61* (16), 7202–7217. https://doi.org/10.1021/acs.jmedchem.8b00557.

(71) Loos, M.; Gerber, C.; Corona, F.; Hollender, J.; Singer, H. Accelerated Isotope Fine Structure Calculation Using Pruned Transition Trees. *Anal. Chem.* **2015**, *87* (11), 5738–5744. https://doi.org/10.1021/acs.analchem.5b00941.

(72) Grinshpun, V.; Rudin, A. Measurement of Mark-Houwink Constants by Size Exclusion Chromatography with a Low Angle Laser Light Scattering Detector. *Makromol. Chem., Rapid Commun.* **1985**, *6* (4), 219–223. https://doi.org/10.1002/marc.1985.030060401.

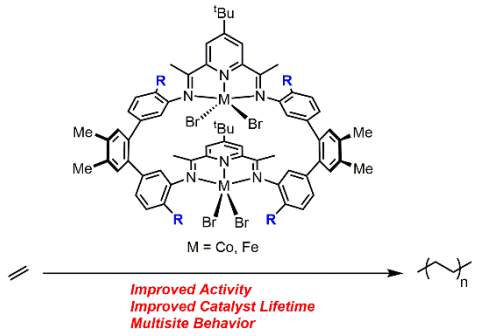
tBu
R
N
M
N
R
Br
Br
tBu
Me
Me
Me
Me
N
M
N
R
Br
Br
R
M = Co, Fe
n
Improved Activity
Improved Catalyst Lifetime
Multisite Behavior